NASA TECHNICAL NOTE

NASA TN D-2576

c. 1

TECH LIBRARY KAFB, NM
0079737

NASA TN D-2576

SUPERSONIC INVESTIGATION OF A SPINNING AND NONSPINNING MODEL OF A CAJUN (OR APACHE) ROCKET VEHICLE WITH ROLL-CONTROL TABS

by Ralph A. Falanga

Langley Research Center
Langley Station, Hampton, Va.

NATIONAL AERONAUTICS AND SPACE ADMINISTRATION • WASHINGTON, D. C. • JANUARY 1965

TECH LIBRARY KAFB, NM

0079737

SUPERSONIC INVESTIGATION OF A SPINNING AND NONSPINNING MODEL OF A CAJUN (OR APACHE) ROCKET VEHICLE WITH ROLL-CONTROL TABS

By Ralph A. Falanga

Langley Research Center
Langley Station, Hampton, Va.

NATIONAL AERONAUTICS AND SPACE ADMINISTRATION

For sale by the Office of Technical Services, Department of Commerce,
Washington, D.C. 20230 -- Price $2.00

SUPERSONIC INVESTIGATION OF A SPINNING AND NONSPINNING MODEL OF A CAJUN (OR APACHE) ROCKET VEHICLE WITH ROLL-CONTROL TABS

By Ralph A. Falanga
Langley Research Center

SUMMARY

A model of the Cajun rocket with nose cone and standard fin assembly (scaled to 0.401) was tested in the Langley Unitary Plan wind tunnel from Mach numbers of 2.30 to 4.63 at a Reynolds number of 2.5×10^6 per foot. Some additional data are presented for Reynolds number of 4.0×10^6 per foot and for model incidence angles other than zero. Measured wind-tunnel results on 11 roll-control-tab configurations (plates with wedge-shaped cross section) for mounting on the trailing edge of the stabilizing fins of Cajun stage to obtain roll-effectiveness data are presented herein along with the general aerodynamic characteristics defining this vehicle. The data obtained for the total rolling-moment coefficient and the damping-in-roll derivative compared favorably with theoretical results.

INTRODUCTION

The Nike-Cajun (CAN), a two-stage solid-propellant rocket vehicle, jointly developed by NASA and University of Michigan was initially proposed as a meteorological sounding rocket system. For example, CAN systems have been successfully used in free-flight investigations to measure atmospheric densities, winds aloft, and even used to photograph hurricanes. These missions were successful as long as CAN, with its initially designed hardware (now considered standard) and with a reasonable amount of static margin, flew zero-lift and nonspinning trajectories. Any required vehicle maneuver which induced loadings beyond the scope outlined, however, would warrant careful analysis of vehicle dynamics before the system is considered flight-worthy. Recently, some standard CAN systems have been spun-up in flight either to satisfy payload requirements or for range safety reasons and the outcome for some flights resulted in vehicle motions which were unexpectedly large. For example, some systems went unstable, and coned through large angles; others had their flights terminated abruptly because of structural failure. Moreover, in most flights the spin velocities were not in agreement with preflight calculations. Apparently then, either the estimates of the vehicle aerodynamic coefficients were not adequate for more favorable correlation with flight results or else, because of aeroelastic

effects, the structural integrity of the system was being exceeded to cause these unpredicted results.

Since a frequent maneuver request on the Cajun or Apache rocket stage (the Apache rocket, incidentally, is geometrically identical to the Cajun rocket and differs only in motor total impulse) has been to spin-up the vehicle for payload requirements and also to maintain a prescribed rolling history, possibly close to the pitch or yaw natural frequency of the system, it appears necessary for assurance of successful mission measurements that more precise aerodynamic characteristics both during spinning and nonspinning maneuvers on the Cajun or Apache stage be available.

The purpose of this investigation was to supplement existing aerodynamic data on the Cajun or Apache stage of the CAN system by undertaking a wind-tunnel investigation on this stage. Measured wind-tunnel results on 11 roll-control-tab (wedge-shaped cross-section) configurations for mounting on the trailing edge of the stabilizing fins to obtain roll-effectiveness data are presented herein along with the general aerodynamic characteristics of this stage. This type of roll-control hardware is presently being used on flight systems.

A model of the Cajun (scaled to 0.401) with nose cone and standard fin assembly was tested in the Langley Unitary Plan wind tunnel from Mach numbers of 2.30 to 4.63 at a Reynolds number of 2.5×10^6 per foot. Some additional data were obtained at Reynolds number of 4.0×10^6 per foot and are also presented herein. The investigation was divided into two phases; one phase was devoted entirely to obtaining measurements on the system under a free-spinning condition and the other phase, a nonrolling condition, to obtain measured forces and moments induced on the model by the various fin tab configurations.

SYMBOLS

The force and moment coefficients are referred to the body-axis system. All aerodynamic moments are taken about the balance pitch center which was located at station 38.84. Symbols used in this paper are defined as follows:

c chord of roll-control tab (see fig. 2(a))

C_A axial-force coefficient excluding base drag, $\frac{\text{Axial force}}{q_\infty S}$, $C_{D_{\alpha=0^\circ}}$

$\left(C_{D,t}\right)_{\alpha=0^\circ}$ total drag coefficient including base drag

$C_{D,b}$ base drag coefficient

C_l rolling-moment coefficient, $\frac{\text{Rolling moment}}{q_\infty S d}$

C_m pitching-moment coefficient, $\frac{\text{Pitching moment}}{q_\infty S d}$

$(C_{m_\alpha})_{\alpha=0^\circ}$ static stability derivative per degree, $\left.\frac{\partial C_m}{\partial \alpha}\right|_{\alpha=0^\circ}$

C_N normal-force coefficient, $\frac{\text{Normal force}}{qS}$

$(C_{N_\alpha})_{\alpha=0^\circ}$ slope of normal-force curve per degree, $\left.\frac{\partial C_N}{\partial \alpha}\right|_{\alpha=0^\circ}$

C_{l_p} damping-in-roll derivative per radian, $\frac{\partial C_l}{\partial\left(\frac{pd}{2V_\infty}\right)}$

$\frac{pd}{2V_\infty}$ roll-effectiveness parameter, radians

d model cylindrical diameter, 0.222 ft

h height of fin roll-control-tab wedge, in. (see fig. 2(a))

M_∞ free-stream Mach number

p rolling velocity, radians/sec

q_∞ free-stream dynamic pressure, lb/sq ft

R_∞ free-stream Reynolds number per foot

S cross-sectional area of model cylindrical section, 0.0388 sq ft

V_∞ free-stream velocity, ft/sec

x distance measured aft from station 0 along model center line, ft

α incidence angle of model center line, deg

δ fin roll-control-tab wedge half-angle, deg (see fig. 2(a))

Subscripts:

cp center of pressure

cg center of gravity

Dots over symbols indicate derivatives with respect to time.

APPARATUS AND METHODS

Test Facility

The tests were conducted in the Langley Unitary Plan wind tunnel at Mach numbers of 2.30 to 4.63 and at free-stream Reynolds numbers of 2.5×10^6 and 4.0×10^6 per foot. This facility is a variable-pressure, continuous, return flow tunnel with two test sections 4 feet square and approximately 7 feet in length. An asymmetric sliding-block nozzle provides a means to vary the Mach number continuously from 1.4 to 2.9 in the low Mach number test section and from 2.3 to 4.7 in the high Mach number test section. The high Mach number test section was used exclusively for these tests. See reference 1 for more details on this tunnel facility.

Models

Photographs of the basic model used in this investigation are shown in figure 1. This model is a 0.401-scaled version of the Cajun stage of CAN system presently being utilized extensively in free-flight studies. A drawing of this model with detail dimensions is shown in figure 2. Eleven different sets (four to a set) of fin-trailing-edge roll-control tabs have been investigated with the basic model. Figure 2(a) gives the important geometric parameters and dimensions necessary to define these roll-control tabs. The basic model was constructed from 2024-T4 aluminum, and a portion of the midsection of the main cylinder (namely, from stations 28.50 to 40.75), the fins, and the roll-control tabs were constructed from 4160 stainless steel. All external fairings on the full-scale Cajun have also been incorporated into the basic model in order that the external-flow-field characteristics be similar. Figures 2(b) and 2(c) illustrate with sketches the internal arrangements of components used in the free-spinning and nonspinning phases of the wind-tunnel program. Sketch (b) of figure 2 illustrates the arrangement of the bearings and spindle necessary to allow the model to spin freely in order to measure the roll effectiveness of the fin roll-control tabs investigated. Sketch (c) illustrates the arrangement of the six-component strain-gage balance used to measure the developed forces and moments from the fin control tabs during the nonrolling phase. The model was mass-balanced dynamically for the free-spinning phase of the program. Eleven different sets of roll-control tabs were tested on the basic model and instead of designating each new set used with the model as a new configuration, the base chord c of the roll-control tab (which has a wedge cross section) and the wedge half-angle δ are used to identify the measured data for the basic model plus tabs presented herein. These geometric parameters, chord and wedge angle, of the control tab are considered primary and completely defined the tabs. (See fig. 2 for specific numbers.)

Test Conditions and Procedure

The tests were performed at Mach numbers of 2.30, 2.96, 3.95, and 4.63, and free-stream Reynolds number of 2.5×10^6 per foot. Some of the tests listed

have been repeated for an increase of 60 percent in free-stream Reynolds number or 4.0×10^6 per foot in order to establish some level of dominance of this parameter for the results obtained. Besides the data obtained at zero incidence, some data have been obtained at incidence angles of $\pm 2^\circ$, $\pm 4^\circ$, and $\pm 6^\circ$. These data, however, are not presented herein in their complete raw form; instead, limited data are used to establish some typical trends with the other measured results and indirectly to establish rates of change with respect to these angles of incidence, for example, C_{N_α} and C_{m_α}. The data reduction will be discussed in more detail in the following section.

The program conducted in the Langley Unitary Plan wind tunnel consisted of two phases: phase 1, the model was allowed to spin freely to an equilibrium, steady-state rolling velocity which was measured with a stroboscope; phase 2, the model had been equipped with six-component strain-gage balance, mounted internally to measure forces and moments for the nonrolling condition. Base-pressure measurements were also made in phase 2. For phase 1, 16-millimeter movies were taken in order to record any abnormal or unpredicted events during free spinning of the model as well as to represent backup data for measuring steady-state spinning velocities. Some exploratory schlieren photographs of the flow field about the aft section of the model were taken during phase 2. Because of the limited view of the flow field obtained for all Mach numbers investigated, a qualitative analysis could not be justified; therefore, these photographs are not presented herein.

Data Reduction and Method of Analysis

All force and moment data have been reduced to coefficient form and referenced to the basic body diameter (0.222 foot) and to the cross-sectional area of the referenced diameter. Also, force and moment coefficients are referred to the body-axis system. The pitch moment center of the balance was located at station 38.84. (The center-of-gravity position occurs at 57 percent of the body length and duplicates the center-of-gravity position of a recent free-flight test of the Cajun stage of a CAN system.)

The static-margin data presented herein, in terms of reference diameter, have been obtained by expressing as a ratio, at zero incidence, the static stability derivative $\left(C_{m_\alpha}\right)_{\alpha=0^\circ}$ to the normal-force slope $\left(C_{N_\alpha}\right)_{\alpha=0^\circ}$; namely, $\frac{x_{cp} - x_{cg}}{d} = -\left.\frac{C_{m_\alpha}}{C_{N_\alpha}}\right|_{\alpha=0^\circ}$. The rolling-velocity data obtained from phase 1 have been reduced to a roll-effectiveness parameter $\frac{pd}{2V_\infty}$; this parameter is in a convenient form from the standpoint that it appears in the rolling-moment equation used to evaluate the model damping-in-roll parameter C_{l_p}. The damping-in-roll derivative was reduced from the measured data by dividing the total rolling-moment coefficient C_l by the roll-effectiveness parameter $\frac{pd}{2V_\infty}$.

The base drag coefficients were obtained from pressure measurements made in the base cavity as well as in the base annulus of the model. The base drag of the cavity region and that of the base annulus were computed separately and then summed to represent the total base drag coefficient presented herein.

Accuracy

The force and moment coefficient data obtained from the six-component strain-gage balance have been corrected for flow angularities and for balance and sting deflections under load. With the fin roll-control tabs removed and the model at zero incidence, no residual roll was observed for the range of test variables studied.

The accuracy of the individual measured quantities, based on calibrations and repeatability of data for these tests is estimated to be within the following limits:

C_N	±0.100
$(C_D)_{\alpha=0^\circ} \equiv C_A$	±0.020
C_m	±0.050
C_l	±0.010
α, deg	±0.100
M_∞	±0.015

For phase 1 with model free spinning, the internal friction contributed by the bearings to the measured data was found to be 1 percent or less of the measured spin rate for all conditions studied, except for the tab, $\delta = 16^\circ$ and $c = 0.615$ inch, at $M = 4.63$ where the error amounted to 4 percent of the measured value of spin velocity. The internal friction for the system was determined from laboratory calibration and a detail description of this calibration is given in the appendix. The stroboscope used to measure steady-state rolling velocity had a range of 110 to 25,000 flashes per minute and the frequency dial was calibrated to 1 percent of all scales.

The damping-in-roll derivatives C_{l_p} reduced from data for the measured total rolling-moment coefficient and roll-effectiveness parameter $\frac{pd}{2V_\infty}$ were estimated to be accurate within the following limits: at $M_\infty = 2.30$, C_{l_p} has an accuracy of ±2.5/radian and at $M_\infty = 4.63$, C_{l_p} has an accuracy of ±10.0/radian. (This accuracy number also includes bearing contributions.)

Aeroelastic effects from the fins at maximum tunnel dynamic pressure were measured in the laboratory by superimposing static loads calculated for loads induced by spinning and those due to the roll-control tab. The resulting measured deflections were negligible and no corrections were necessary to the wind-tunnel data.

RESULTS AND DISCUSSION

Roll-Effectiveness Parameters

The roll-effectiveness parameters were measured under steady-state conditions and, as illustrated in figures 3 to 7, are for zero-lift conditions. Furthermore, the effect of angle of attack is small as illustrated by the typical plot of this effect in figure 7. Another small effect on $\frac{pd}{2V_\infty}$ was the slight increase in this parameter as the free-stream Reynolds number was increased from 2.5×10^6 to 4.0×10^6 per foot. This effect of Reynolds number apparently results from the fact that the boundary-layer thickness on a flat plate decreases as Reynolds number to the -1/5th or -1/7th power for turbulent boundary layer (ref. 2). As a result of the decrease in boundary-layer thickness, the roll-control-tab geometries become more effective. However, the effect from Reynolds number appears to predominate at the higher free-stream Mach numbers, that is, essentially above $M = 3.0$. The effect from the nonlinearity portion of the curves shown in figures 5 and 6 is to prevent the roll-effectiveness parameter from changing proportionately with either c or δ. This effect, however, is expected since, even from inviscid theory, the pressure distribution over the wedge surface is expected to vary with wedge half-angle in a similar manner.

Rolling-Moment Coefficient

The rolling-moment coefficient C_l presented in figures 8 to 13 represents the total rolling-moment coefficient of the model due to four roll-control tabs, one tab located on the trailing edge of each of four fins. The C_l data for roll-control tabs with $c = 0.308$ inch and $\delta = 17^\circ$ and with $c = 1.230$ inches and $\delta = 8^\circ$ were not obtained. However, the C_l variation with M_∞ can be obtained for these controls by cross plotting the data presented in figures 10(a) and 10(c), respectively.

Effect of Reynolds number and model incidence angle appear to be slight (within the measured data accuracy) on C_l as illustrated by the trends of the data presented in figures 9 and 12, respectively.

Examination of the rolling-moment data presented in figures 8 to 12 does not indicate the occurrence of any severe flow separation about the roll-control tabs. If any existed, C_l would display some independence with free-stream Mach number. Thus, the omission of such a trend in these data indicates small to negligible effects of flow separation on C_l. According to reference 3, the control tab most likely to succumb to flow separation was the tab with $c = 0.308$ inch and $\delta = 22^\circ$ at M_∞ of 2.30 and 2.96, but this result is not substantiated by these data.

Comparisons of theoretical C_l values with experimental values are shown in figure 13. The comparisons were made for the various roll-control-tab chords

investigated and for roll-control-tab angle of 12°. The theories used were both two dimensional and inviscid and excluded any body effects or interference effects from body on tabs. One theory utilized was Busemann's small perturbation theory where the pressure coefficient equation was linearized by evaluating only the first term of the series expression, namely, $\frac{\Delta p}{q_\infty} = \frac{2\delta}{\sqrt{M_\infty^2 - 1}}$. (See ref. 4.) The other theoretical results shown in these plots represent oblique shock results from compressible flow charts of reference 5. In general, Busemann's linearized results appear to be the better fit of the two theories with the experimental data. However, for the longest chord investigated, c = 1.230 inches, Busemann's linearized results underpredict the experimental data by as much as the results obtained by using reference 5 overpredict them.

Damping-in-Roll Parameter

The C_{l_p} values reduced from the data obtained from the free-spinning phase and nonspinning phase of the wind-tunnel program are presented in figure 14 for the roll-control tabs, except for omission of those data of C_l mentioned previously. The trend exists that for each roll-control chord, the C_{l_p} values were highest for the largest tab angle and decreased with decreasing tab angle. The spread due to tab angle change in C_{l_p} values for a given chord increased as the free-stream Mach number increased. Some of this spread appears to be associated with the accuracy of these data. As was mentioned in the section "Accuracy," C_{l_p} values reduced from the measured C_l and $\frac{pd}{2V_\infty}$ data were less accurate at the higher Mach numbers. The inaccuracies estimated included contributions (1) from internal bearing friction on steady-state rolling velocity, (2) from C_l, and (3) from the deviations in the very low values of roll-effectiveness parameter which existed at the higher Mach numbers of these tests.

Comparisons of theoretical results with experimental C_{l_p} values are presented in figure 15 for the various roll-control-tab chords investigated and for a tab angle of 12°. The theory utilized (ref. 6) was for potential, inviscid flow and for an isolated wing planform. The C_{l_p} values computed from reference 6 were for two fins and were doubled for one case and multiplied by a factor of 1.55 for a second case to obtain representative C_{l_p} values for the four-fin assembly arrangement. For the case where C_{l_p} values were doubled, the assumption was made that fin-fin or fin-body interference effects on C_{l_p} were negligible. Estimates of body interference effects indicated a very small effect on C_{l_p} mainly because the ratio of body diameter to fin span was low for the test model. In the second case, the factor of 1.55 was obtained from reference 7 which included theoretical estimates of interference effects on C_{l_p}. The results developed in reference 7, however, were for a slightly different fin planform, namely, that for a full delta. The results for a clipped delta planform (fins tested herein) were not available. Thus, the factor to convert

C_{l_p} for a two-fin arrangement to that for a four-fin arrangement may lie between 2 and 1.55, apparently closer to 2. The theoretical results with a factor of 2 agreed favorably with the measured data, in fact, these theoretical results represented a mean for the experimental data presented. The theoretical results incorporating the factor of 1.55 underpredicted the experimental data by approximately 20 percent.

Aerodynamic Characteristics

Besides the data pertaining to the model rolling characteristics which have been presented thus far, some model aerodynamic longitudinal stability characteristics have also been measured. These longitudinal data also apply to the lateral plane as well, since the model was symmetrical. The data for the normal-force-curve slope C_{N_α}, the static stability parameter C_{m_α}, static margin $\frac{x_{cp} - x_{cg}}{d}$, and drag coefficient $C_{D_{\alpha=0^\circ}}$ are presented in figures 16 to 22. The model has adequate static stability as indicated by the C_{m_α} and $\frac{x_{cp} - x_{cg}}{d}$ plots shown in figures 17 and 18, respectively. The drag-coefficient data at zero model incidence angle ($\alpha = 0^\circ$) are presented in figures 19 to 21 for the various roll-control tabs including the data for $\delta = 0^\circ$. However, not included in these data are the model base-drag contributions. The base-drag variation with M_∞ has been measured and is shown in figure 22 along with the total-drag-coefficient data which does include base-drag contributions. This total drag coefficient shown in figure 22 was measured without the presence of any roll-control tabs. The contribution to drag from the roll-control tabs investigated may be obtained from figures 19 and 21. Reynolds number effect on drag coefficient appears to be small as illustrated by the plots of figure 20.

Comparison of Computed and Measured Rolling Velocities

A comparison of rolling velocities reduced from free-flight testing of two full-scale Cajun systems (models 1 and 2) with values obtained from preflight trajectory calculations is shown in figure 23. The preflight trajectory calculations used interpolated values of rolling-moment coefficient C_l and damping in roll C_{l_p} reduced from wind-tunnel measurements for roll-control tab of $c = 0.308$ inch and $\delta = 8^\circ$ and used extrapolated values to cover the free-flight Mach number range of approximately 1.50 to 5.50 since the wind-tunnel values ranged from $M_\infty = 2.30$ to $M_\infty = 4.63$. Also, the preflight calculations were based on rigid aerodynamics. The flight results from model 1 agreed favorably with preflight computed values throughout the thrusting and coasting phases whereas the results for flight model 2 differed from those for model 1 by 1 cycle per second and from preflight results by 3/4 cycle per second during the coasting phase. The difference in flight results from the two systems is attributable mainly to an effective 3-minute fin misalinement (preflight measurement) opposing the velocity in roll produced by roll-control tabs. Moreover, by using strip theory (developed for steady-state conditions), this effective

fin misalinement produced an opposing rolling velocity of approximately 1 cycle per second, the approximate amount the flight results differ.

SUMMARY OF RESULTS

Measured wind-tunnel results on 11 roll-control-tab configurations (plates with wedge-shaped cross section) for mounting on the trailing edge of the stabilizing fins of the Cajun stage to obtain roll-effectiveness data are presented herein along with the general aerodynamic characteristics defining this vehicle for the free-stream Mach number range of 2.30 to 4.63 at free-stream Reynolds number of 2.5×10^6 per foot. Some additional data are presented for Reynolds number of 4.0×10^6 per foot and for model incidence angles other than zero. The total rolling-moment-coefficient data are compared with the results from two simple inviscid theories; one theory, Busemann's small perturbation theory, fits the experimental results, in general, better than the results from the oblique-shock theory. The latter theoretical results, in all cases, overpredict the experimental values. The damping-in-roll parameter reduced from wind-tunnel measurements is in agreement with the theoretical results when the damping-in-roll derivatives computed for two fins were doubled for four-fin assembly arrangement. Preflight calculations of rolling-velocity history using present wind-tunnel measurements agree favorably with results from free-flight testing of the full-scale Cajun vehicle. Besides reporting on the aforementioned results, the roll-effectiveness parameter and some model longitudinal aerodynamic coefficients which also apply for the lateral plane as well have been presented herein.

Langley Research Center,
National Aeronautics and Space Administration,
Langley Station, Hampton, Va., September 9, 1964.

APPENDIX

INTERNAL BALL-BEARING FRICTION EVALUATION

The contribution of internal friction from the ball bearings used in phase 1 of the free-spinning model was evaluated in the laboratory by simulating the axial and radial loads experienced by the bearings during wind-tunnel operation. For this laboratory setup the model was stripped of the stabilizing fins to minimize the contribution in this evaluation of aerodynamic damping and the model was then inclined at $34^{\circ}10'$ to the horizontal in order to take advantage of the weight of the model to duplicate for the greatest wind-tunnel free-stream dynamic pressure q_{∞} the axial and radial loads induced on these bearings. (See fig. 24 for model setup.) Next, the model was given an initial spin impulse and the time rate of decay of the rolling velocity was recorded. The resulting history is shown in figure 25.

The roll mass moment of inertia I_X was calculated for this system to be 0.0058 slug-ft^2; differentiation of the curve of figure 25 yields $\dot{p}$; and the resulting torque T associated with $\dot{p}$ and I_X was calculated from the expression

$$T = I_X\dot{p} \tag{1a}$$

The resulting torque T represents the torque of the system which can be reduced to two components, namely, the bearing torque T_b and the external viscous-layer skin frictional torque T_{sf}; thus, T can be expressed as

$$T = T_b + T_{sf} \tag{1b}$$

By using references 2 and 8, the skin frictional torque was evaluated and plotted as a function of revolutions per minute as shown in figure 26. Thus, the bearing torque T_b was evaluated from the torque equation, namely,

$$T_b = T - T_{sf} \tag{1c}$$

In order to illustrate how this bearing torque T_b affects the steady-state rolling velocity, the sequence of equations which follows was employed. For steady-state conditions, the rolling moment gives

$$M_X = \sum \text{moments} \equiv 0 \tag{2}$$

or

$$\sum \text{moments} = M_{af} + M_{ad} + M_{bf} = 0 \tag{2a}$$

where

M_{af} moments due to aerodynamic forcing function

M_{ad} moments due to aerodynamic damping

M_{bf} moments due to bearing friction

Rearranging equation (2a) gives

$$\frac{-M_{ad}}{M_{af}} = 1 + \frac{M_{bf}}{M_{af}} \tag{2b}$$

Expressing the aerodynamic damping moment in derivative form and aerodynamic forcing moment in coefficient form on the left-hand side of equation (2b) gives

$$\frac{-C_{l_p} \frac{pd}{2V_\infty} q_\infty Sd}{C_l q_\infty Sd} = 1 + \frac{M_{bf}}{M_{af}} \tag{2c}$$

and solving for steady-state rolling velocity from equation (2c) gives the expression desired, namely,

$$p = -\frac{C_l}{C_{l_p}}\left(\frac{2V_\infty}{d}\right)\left(1 + \frac{M_{bf}}{M_{af}}\right) \tag{3}$$

Note that in the absence of bearing torque $\left(T_b \equiv M_{bf} = 0\right)$, equation (3) reduces to the common form for roll effectiveness $\frac{pd}{2V_\infty} = -\frac{C_l}{C_{l_p}}$. Equation (3) illustrates that as the bearing torque increases, the correction to p increases by the ratio of $\frac{M_{bf}}{M_{af}}$.

The amount of correction to p measured during wind-tunnel operation is demonstrated by the following example for one condition: namely, $p \geqq 2000$ rpm. From figure 25, $\dot{p} = -17.6$ rpm/sec and from equation (1a) for $I_X = 0.0058$ slug-ft^2 $T = I_X\dot{p} = -0.01068$ ft-lb.

Figure 26 gives $T_{sf} = 0.00078$ ft-lb; therefore, the bearing torque T_b is equal to $T - T_{sf}$ or -0.0099 ft-lb.

For the following wind-tunnel conditions the correction for p may be evaluated:

$$M_\infty = 2.30$$

$$q_\infty = 567 \text{ lb/sq ft}$$

$$M_{bf} = T_b = -0.0099 \text{ ft-lb}$$

$$M_{af} = 4.771 \text{ ft-lb}$$

$$\frac{M_{bf}}{M_{af}} = -0.0021$$

where

$$M_{af} = C_l q_\infty S d$$

and

$$S = 0.0388 \text{ sq ft}$$

$$d = 0.222 \text{ ft}$$

$$c = 1.230$$

$$\delta = 12^\circ$$

$$C_l = 0.975$$

Thus, the correction to p amounts to only 0.21 of a percent and is considered to be negligible; thus, any correction from bearing friction at $M_\infty = 2.30$ was ignored as stated in the accuracy section of this report.

REFERENCES

1. Anon.: Manual for Users of the Unitary Plan Wind Tunnel Facilities of the National Advisory Committee for Aeronautics. NACA, 1956.

2. Schlichting, Hermann (J. Kestin, trans.): Boundary Layer Theory. Fourth ed., McGraw-Hill Book Co., Inc., 1960.

3. Kuehn, Donald M.: Experimental Investigation of the Pressure Rise Required for the Incipient Separation of Turbulent Boundary Layers in Two-Dimensional Supersonic Flow. NASA MEMO 1-21-59A, 1959.

4. Busemann, A.: Aerodynamic Lift at Supersonic Speeds. Ae. Techl. 1201, Rep. No. 2844, British A.R.C., Feb. 3, 1937. (From Luftfahrtforschung, Bd. 12, Nr. 6, Oct. 3, 1935, pp. 210-220.) (Also available as Translation No. 196, Douglas Aircraft Co., Inc.)

5. Ames Research Staff: Equations, Tables, and Charts for Compressible Flow. NACA Rep. 1135, 1953. (Supersedes NACA TN 1428.)

6. Harmon, Sidney M.; and Jeffreys, Isabella: Theoretical Lift and Damping in Roll of Thin Wings With Arbitrary Sweep and Taper at Supersonic Speeds - Supersonic Leading and Trailing Edges. NACA TN 2114, 1950.

7. Adams, Gaynor J.; and Dugan, Duane W.: Theoretical Damping in Roll and Rolling Moment Due to Differential Wing Incidence for Slender Cruciform Wings and Wing-Body Combinations. NACA Rep. 1088, 1952.

8. Theodorsen, Theodore; and Regier, Arthur: Experiments on Drag of Revolving Disks, Cylinders, and Streamline Rods at High Speeds. NACA Rep. 793, 1944. (Supersedes NACA ACR L4F16.)

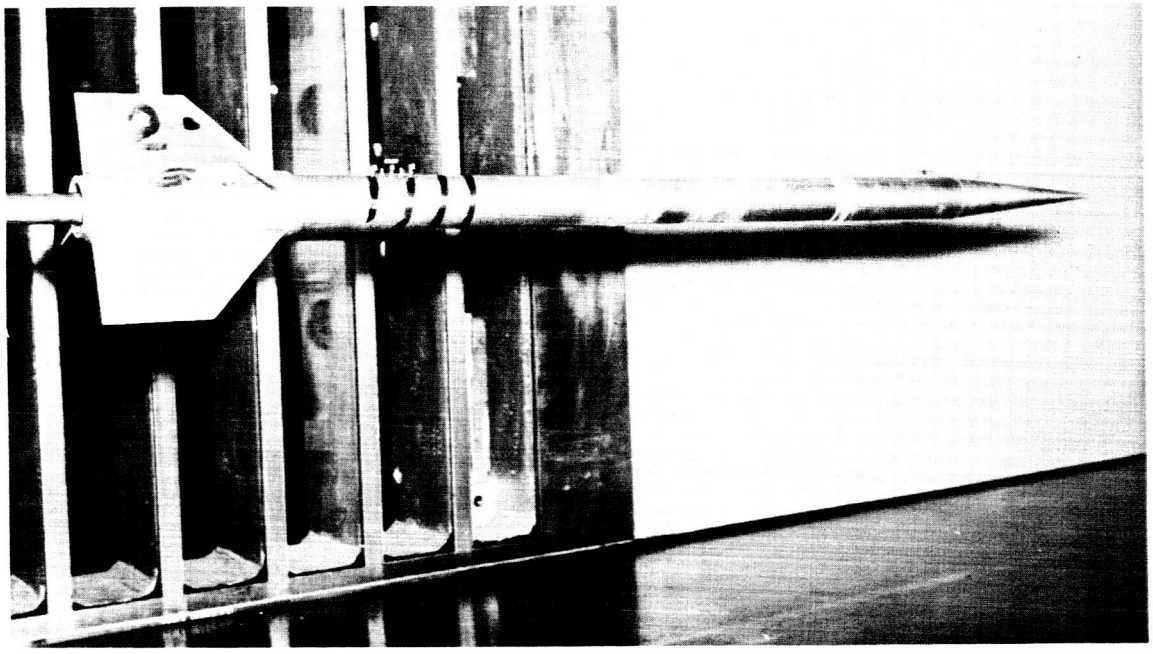

(a) Model mounted with ball bearings on wind-tunnel sting.

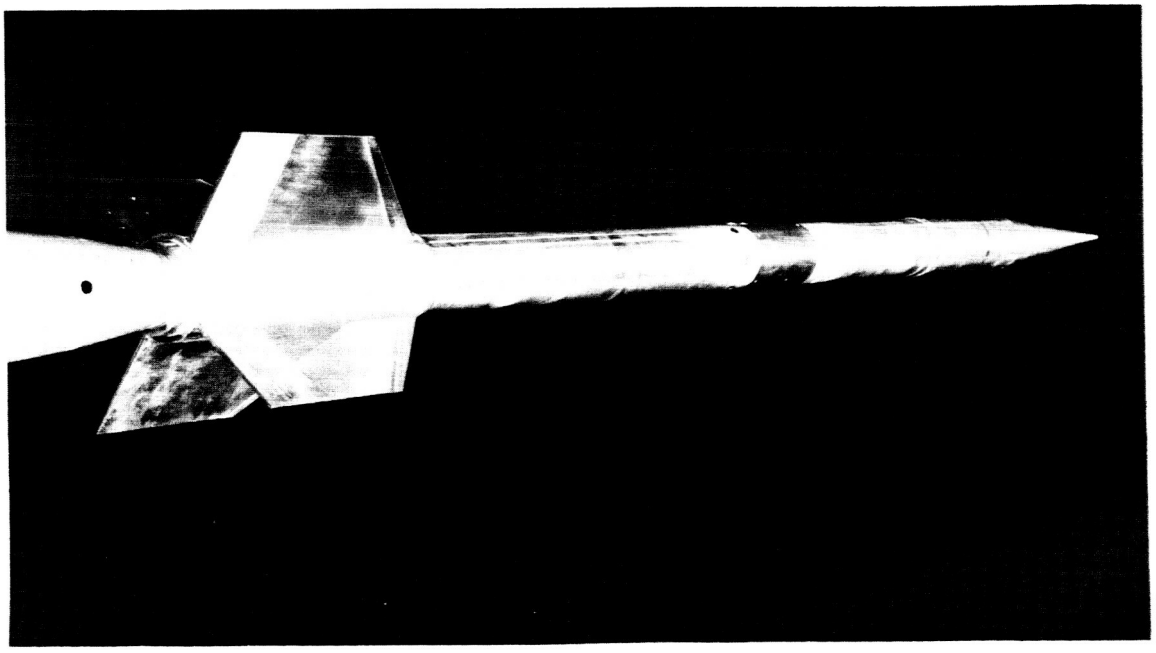

(b) Model mounted with strain-gage balance on wind-tunnel sting. L-64-8327

Figure 1.- Photographs of model arrangements used in wind-tunnel investigation.

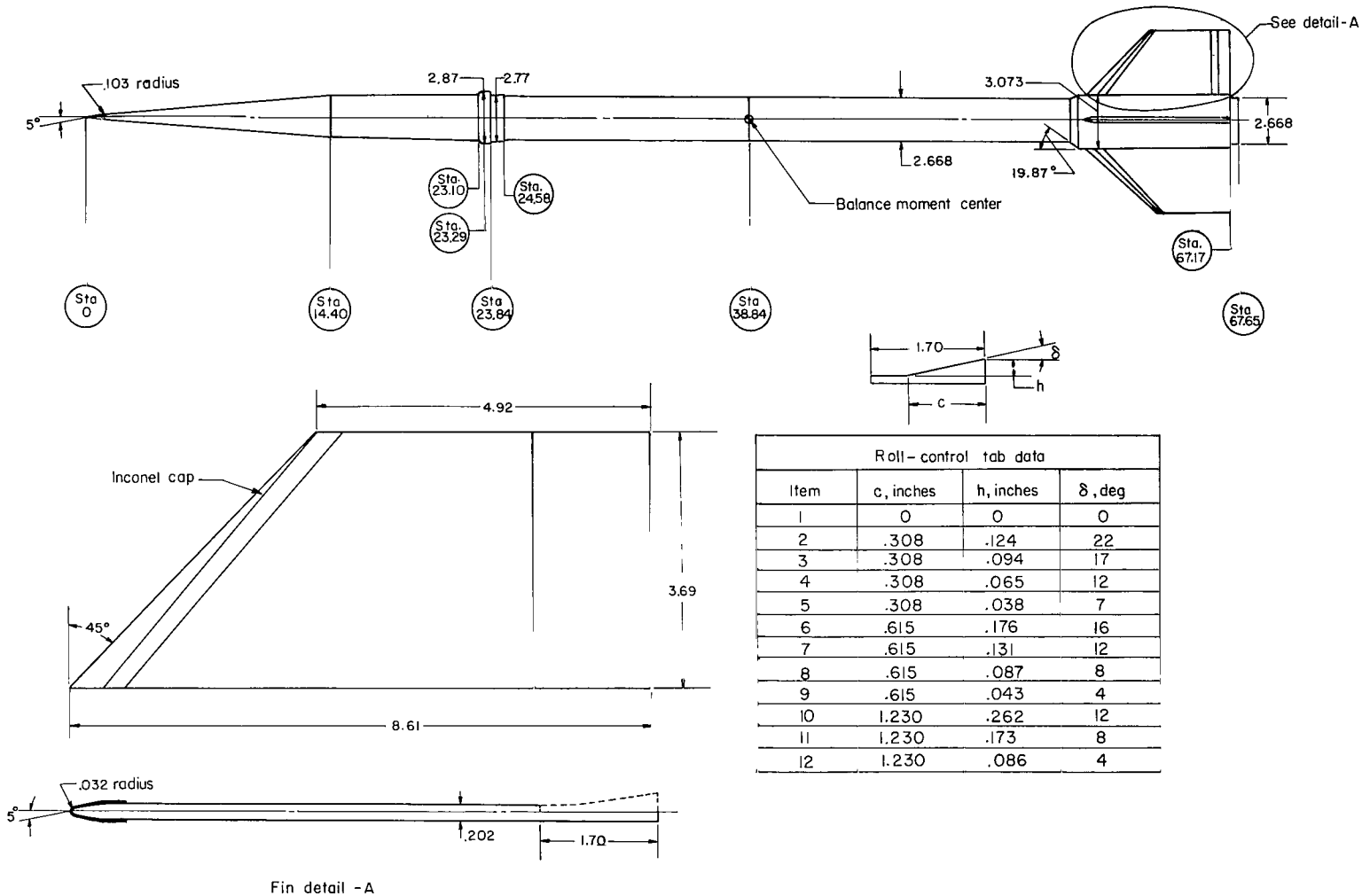

Roll-control tab data			
Item	c, inches	h, inches	δ, deg
1	0	0	0
2	.308	.124	22
3	.308	.094	17
4	.308	.065	12
5	.308	.038	7
6	.615	.176	16
7	.615	.131	12
8	.615	.087	8
9	.615	.043	4
10	1.230	.262	12
11	1.230	.173	8
12	1.230	.086	4

(a) Detail of model and roll-control tabs.

Figure 2.- Detail dimensions of model including table of roll-control data and arrangement of internal components. (All dimensions are in inches unless otherwise noted.)

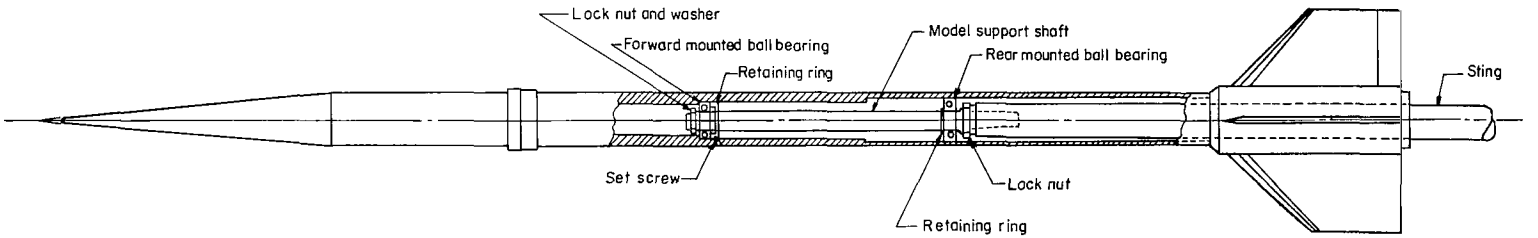

(b) Detail of model mounted on ball-bearing spindle and sting support.

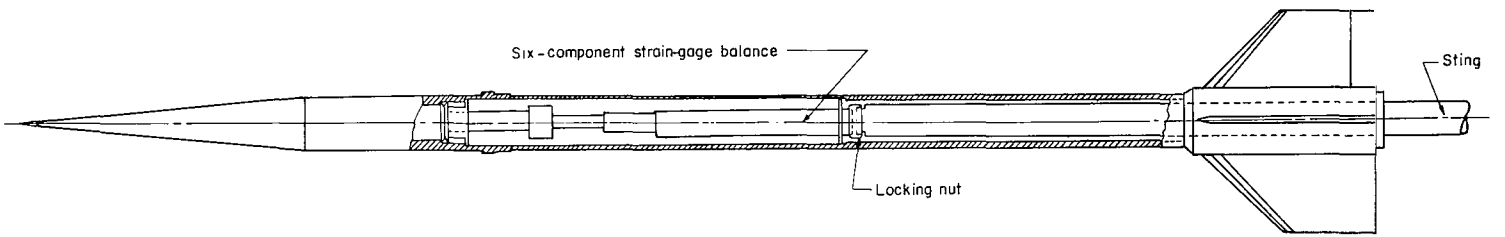

(c) Detail of model mounted on six-component strain-gage balance and sting support.

Figure 2.- Concluded.

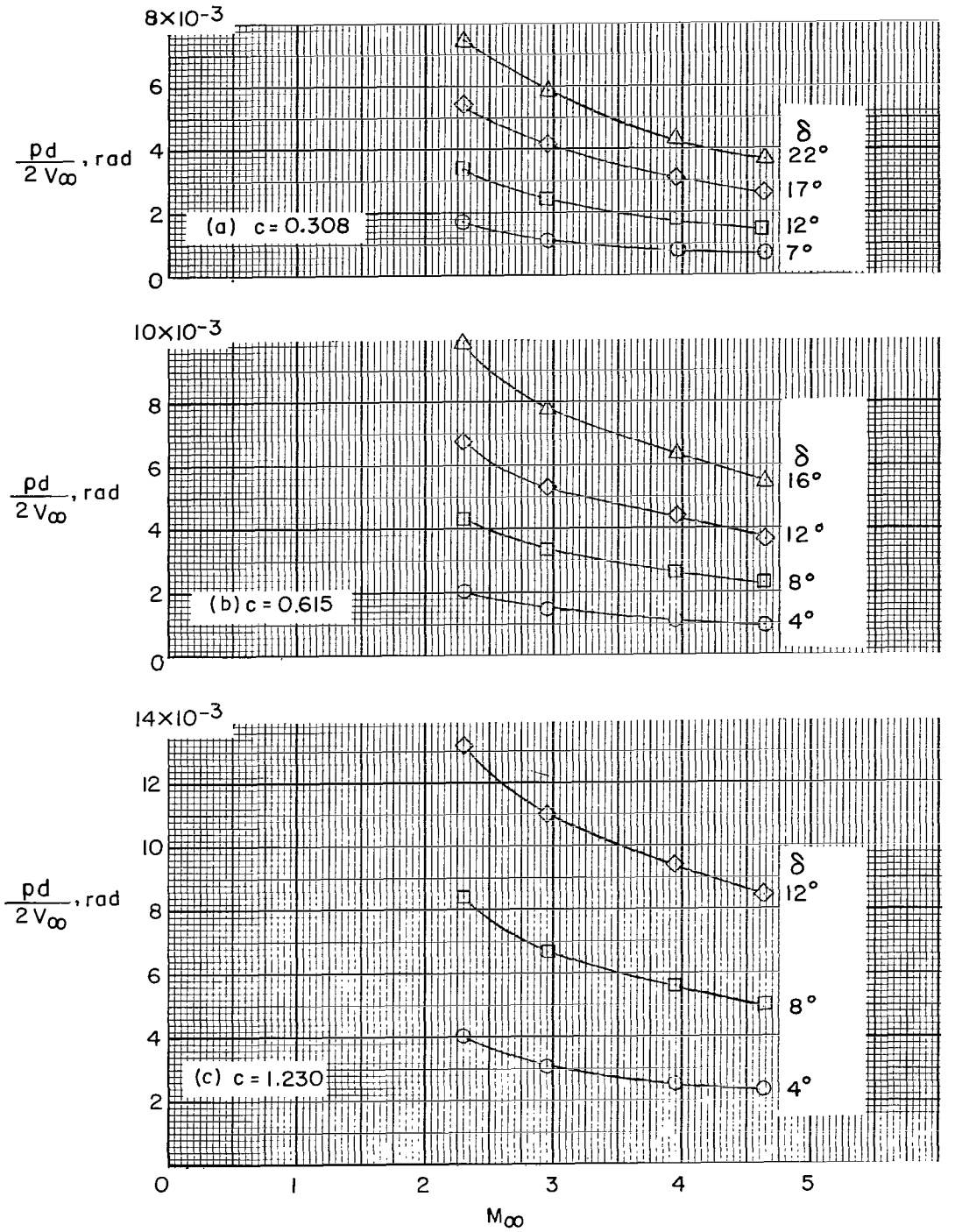

Figure 3.- Variation with free-stream Mach number of roll-effectiveness parameter $\frac{pd}{2V_\infty}$ for all roll-control tabs investigated.

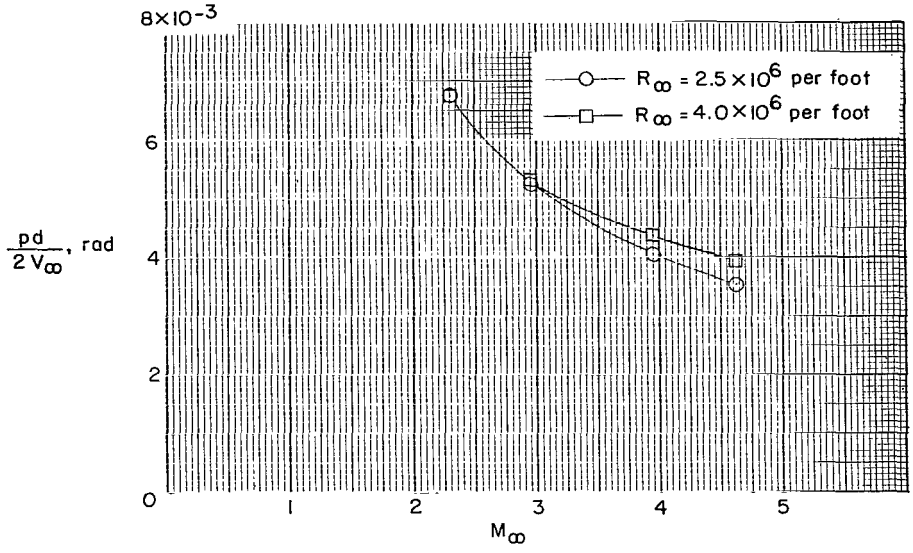

(a) $c = 0.615$; $\delta = 12^{\circ}$.

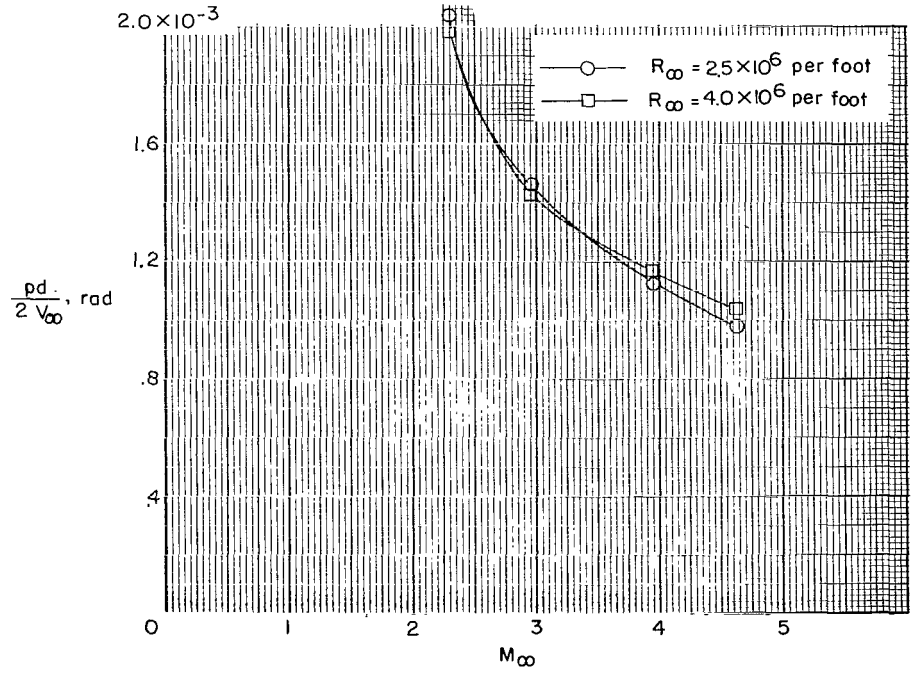

(b) $c = 0.615$; $\delta = 4^{\circ}$.

Figure 4.- Effect of Reynolds number on roll-effectiveness parameter $\frac{pd}{2V_{\infty}}$ for roll-control tabs with $c = 0.615$; $\delta = 4^{\circ}$ and 12°.

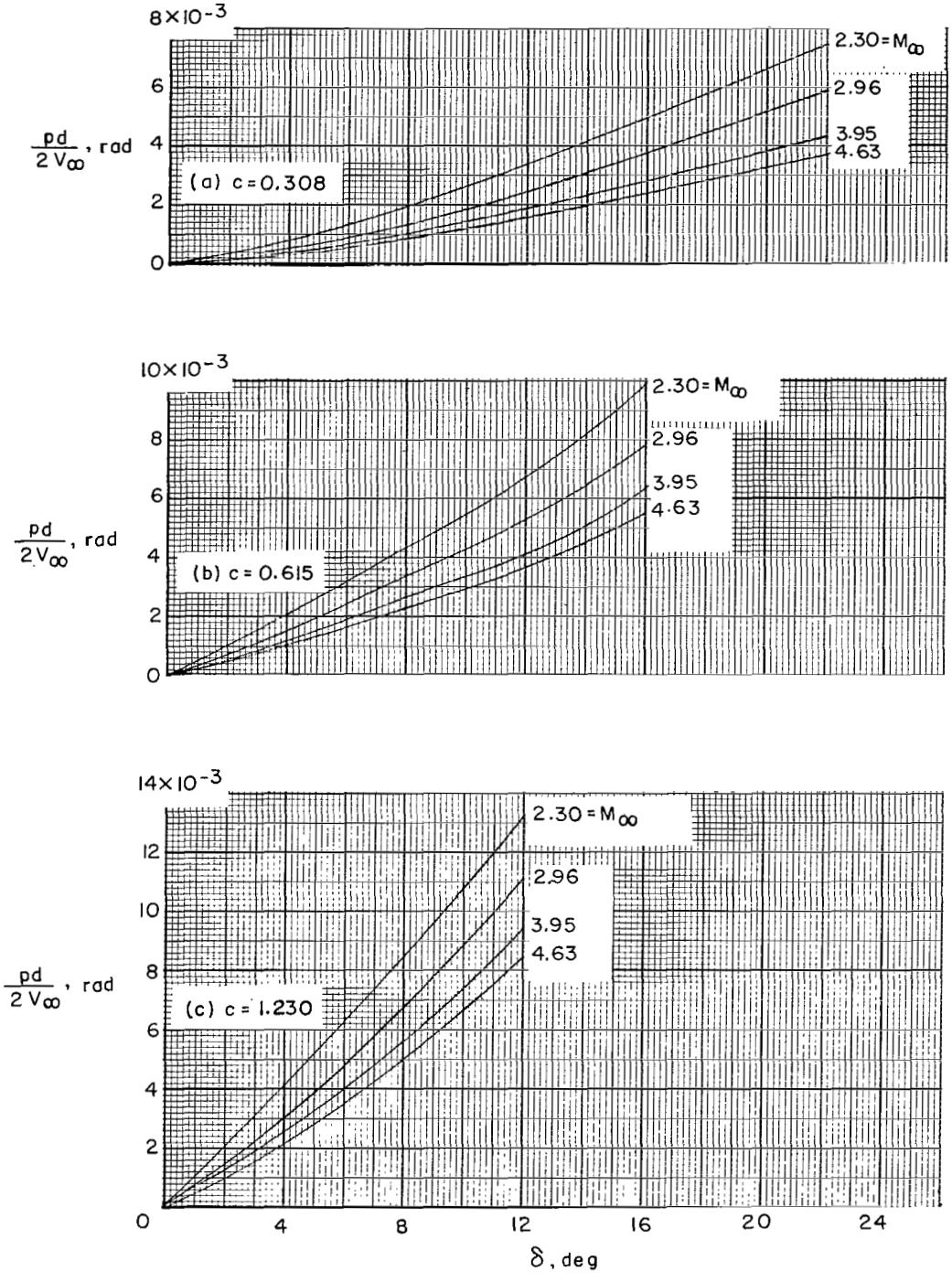

Figure 5.- Variation of roll-effectiveness parameter $\frac{pd}{2V_\infty}$ with roll-control-tab wedge angle δ for free-stream Mach numbers investigated.

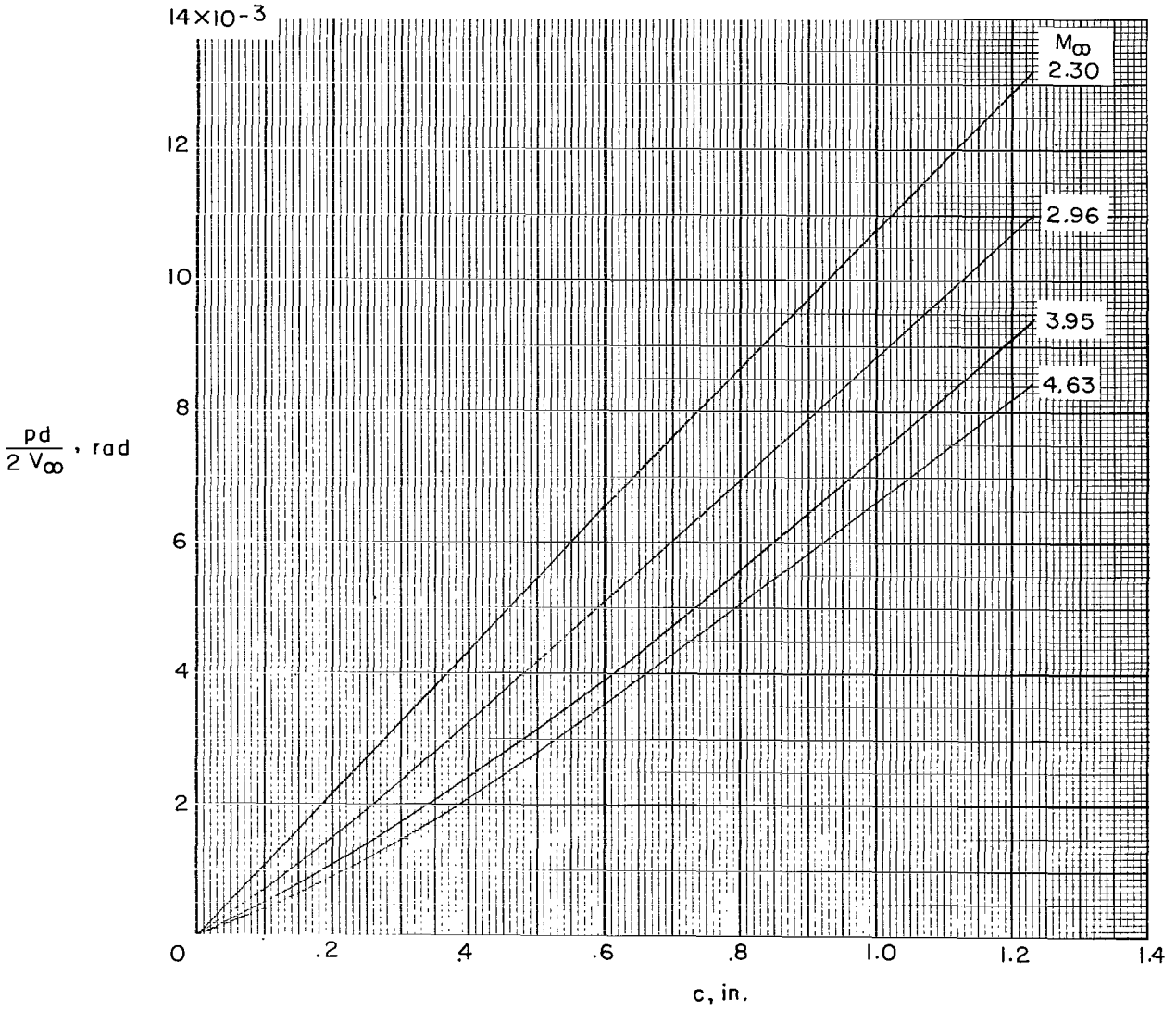

Figure 6.- Variation of roll-effectiveness parameter $\frac{pd}{2V_\infty}$ with roll-control wedge chord for δ fixed at 12° for free-stream Mach numbers.

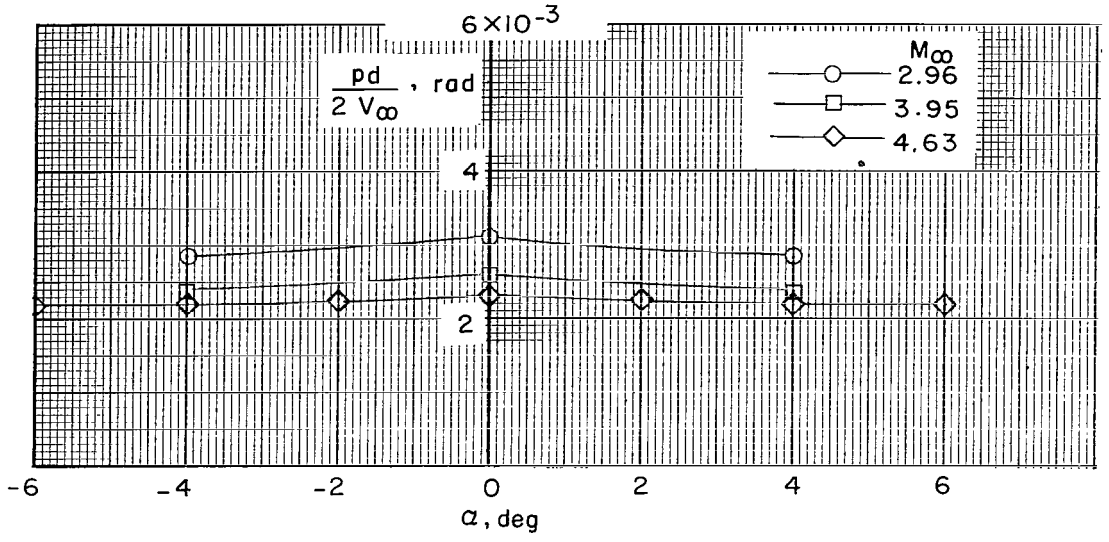

(a) c = 1.23; δ = 4°.

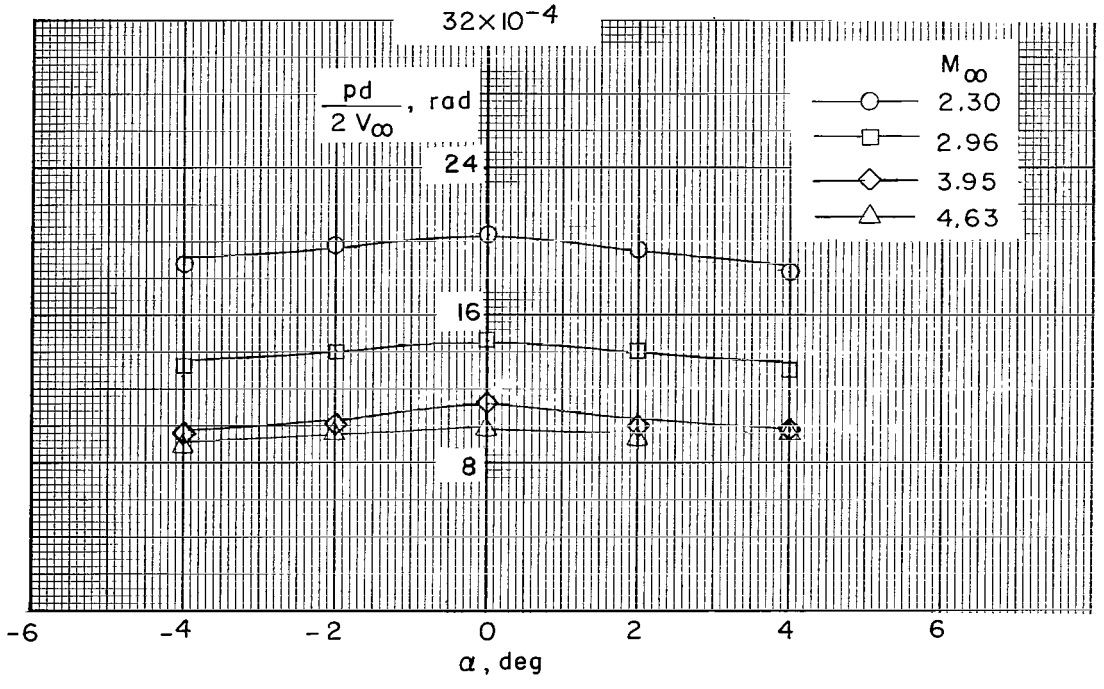

(b) c = 0.615; δ = 8°.

Figure 7.- Typical variation of roll-effectiveness parameter $\frac{pd}{2V_\infty}$ with model incidence angle α for roll-control tabs of $c = 1.23$, $\delta = 4^\circ$ and $c = 0.615$, $\delta = 8^\circ$.

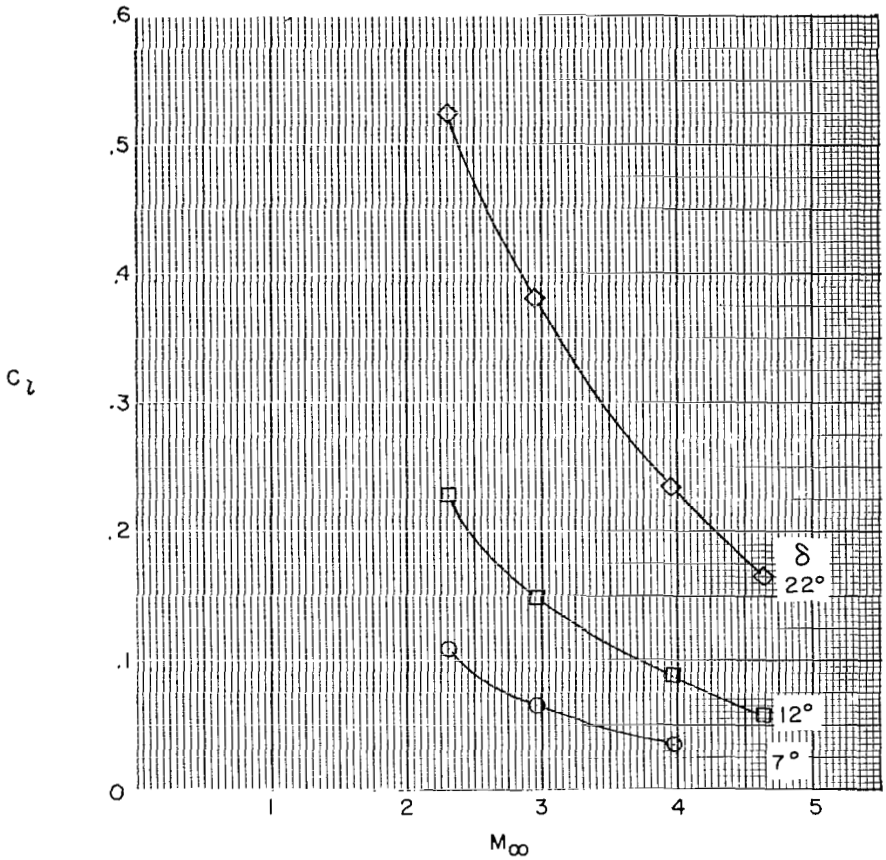

(a) c = 0.308.

Figure 8.- Variation of rolling-moment coefficient with free-stream Mach number for roll-control tabs.

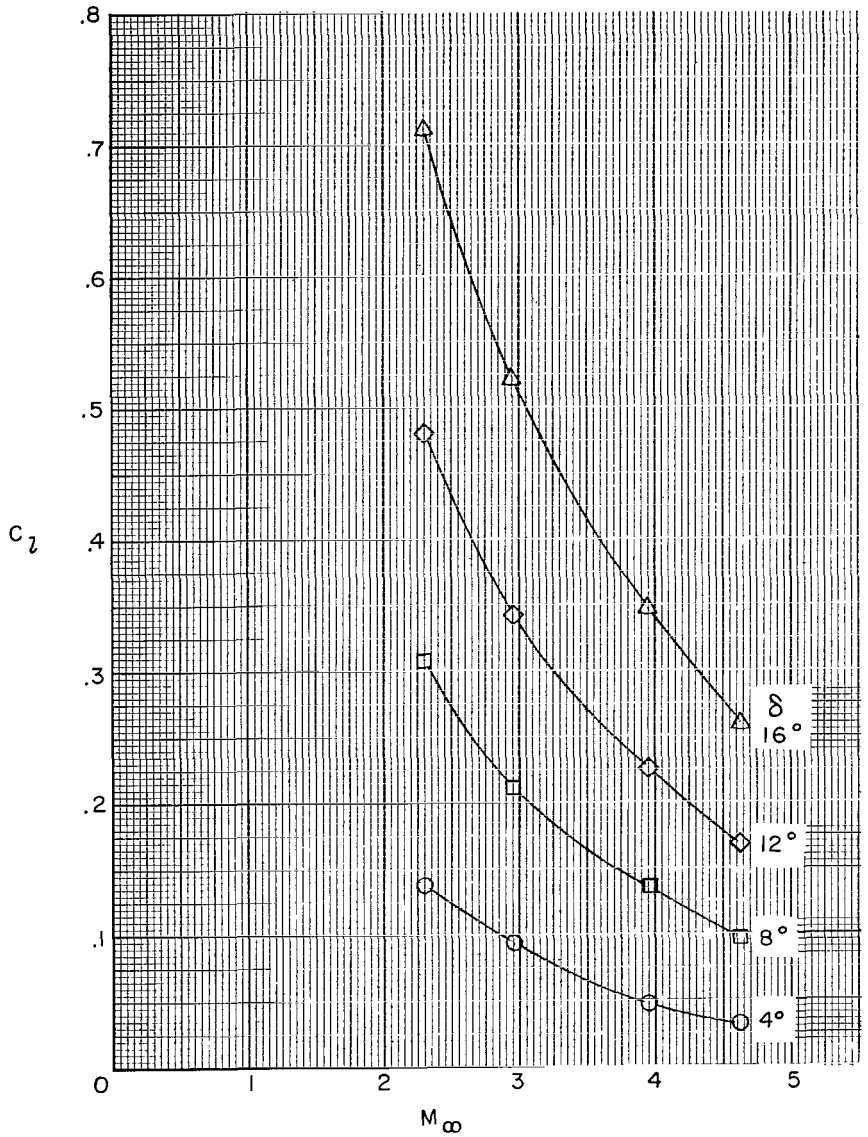

(b) c = 0.615.

Figure 8.- Continued.

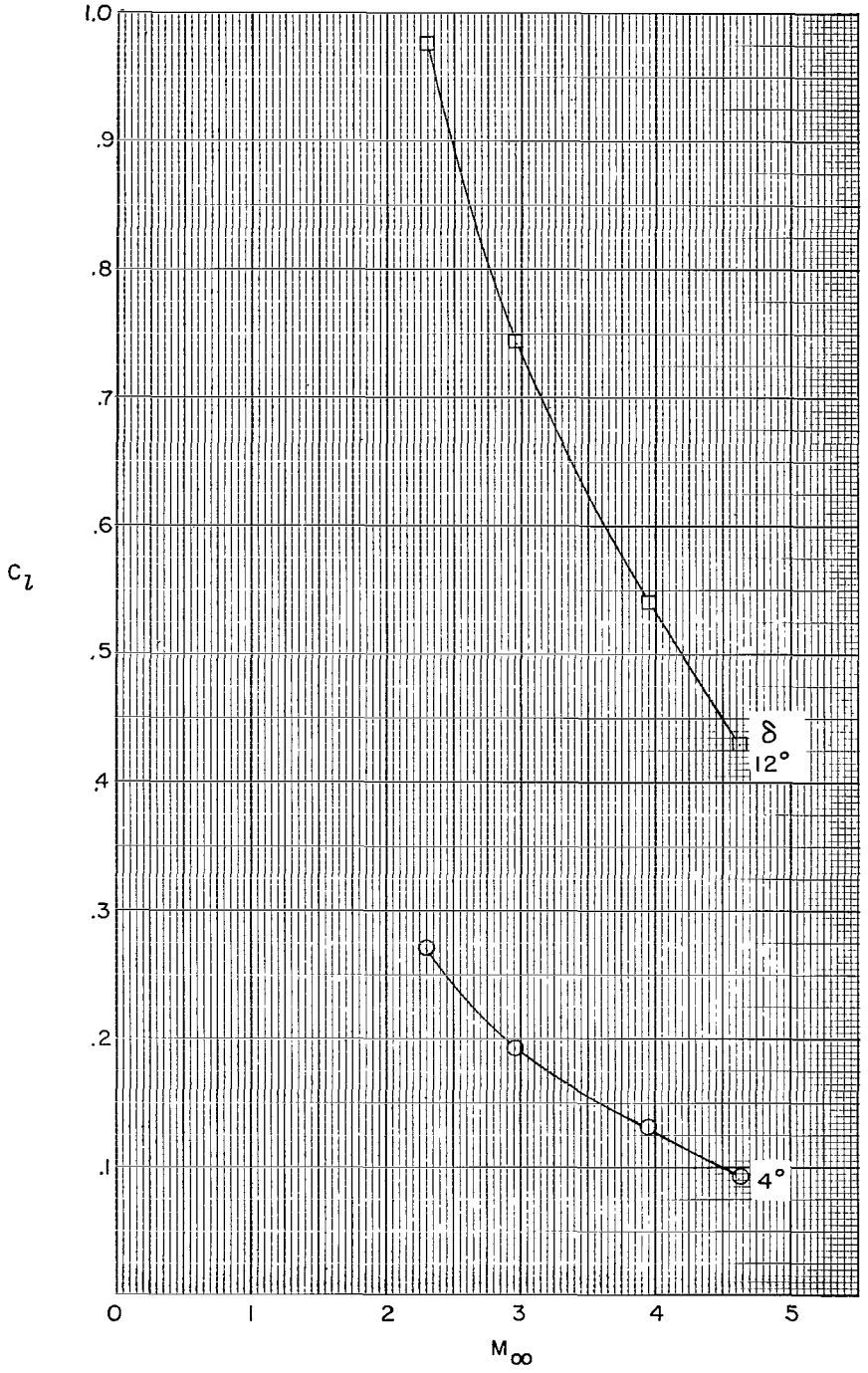

(c) c = 1.230.

Figure 8.- Concluded.

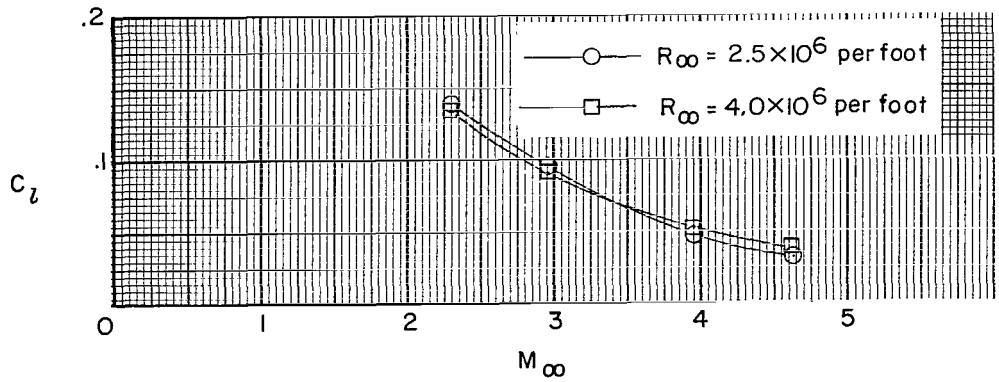

(a) $c = 0.615$; $\delta = 4^\circ$.

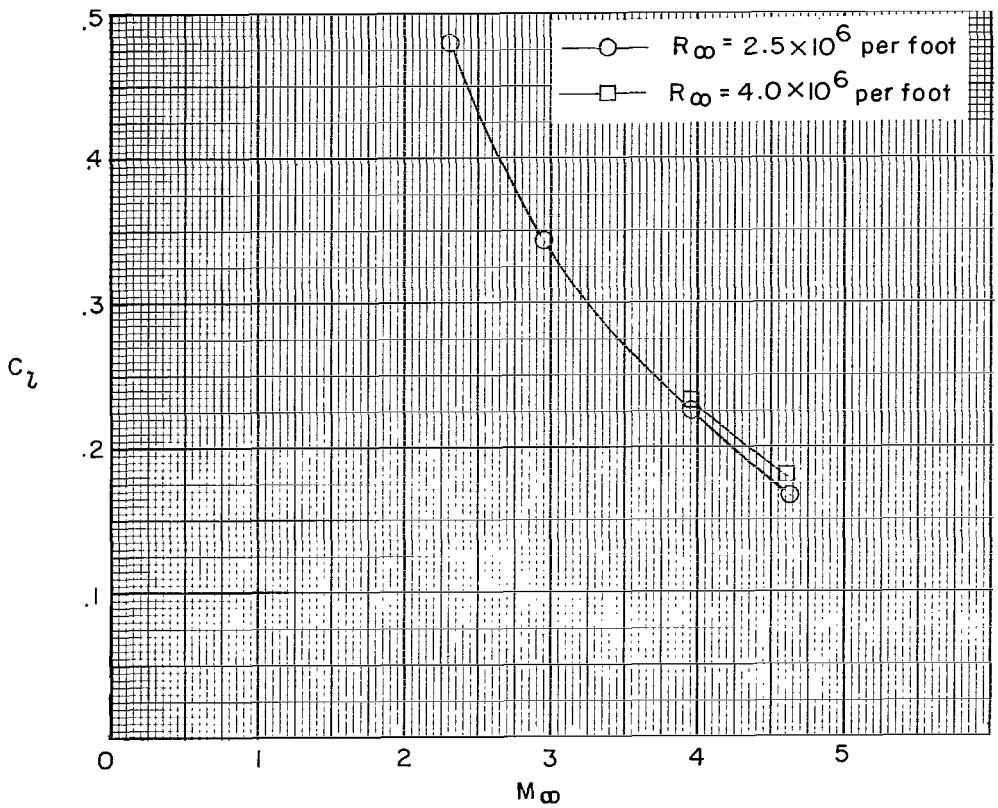

(b) $c = 0.615$; $\delta = 12^\circ$.

Figure 9.- Effect of free-stream Reynolds number on rolling-moment coefficient for control tab of $c = 0.615$ and $\delta = 4^\circ$ and 12°.

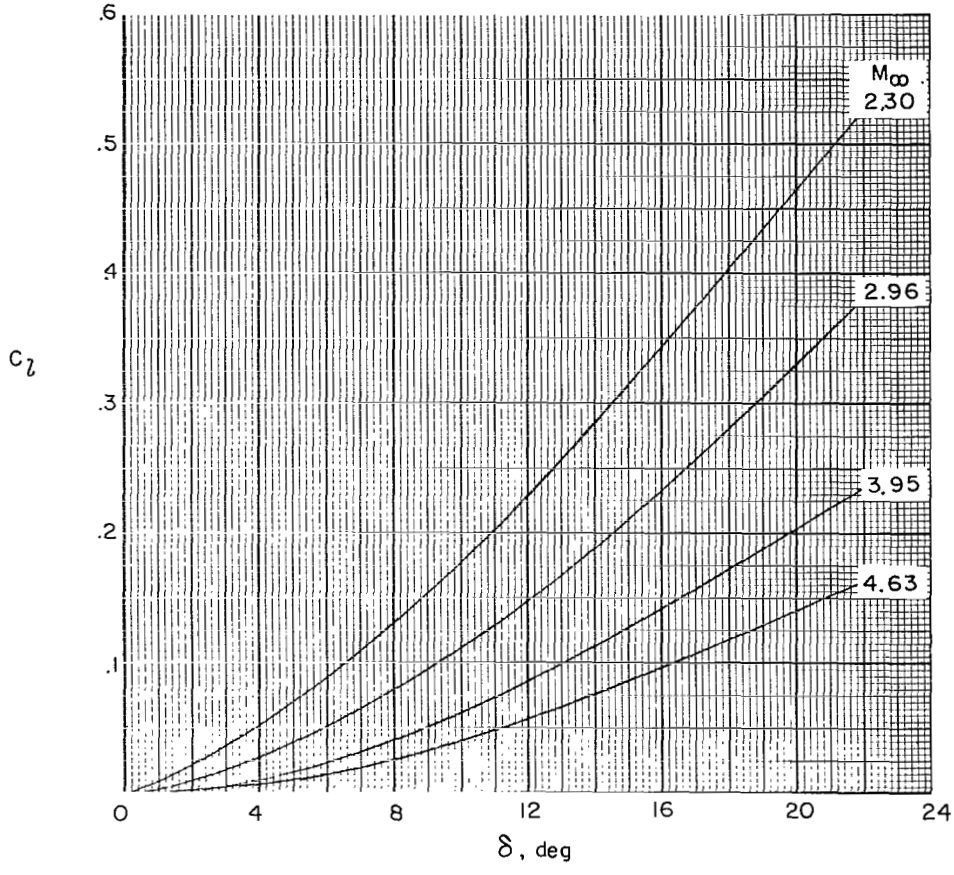

(a) c = 0.309.

Figure 10.- Variation of rolling-moment coefficient with roll-control-tab wedge angle δ.

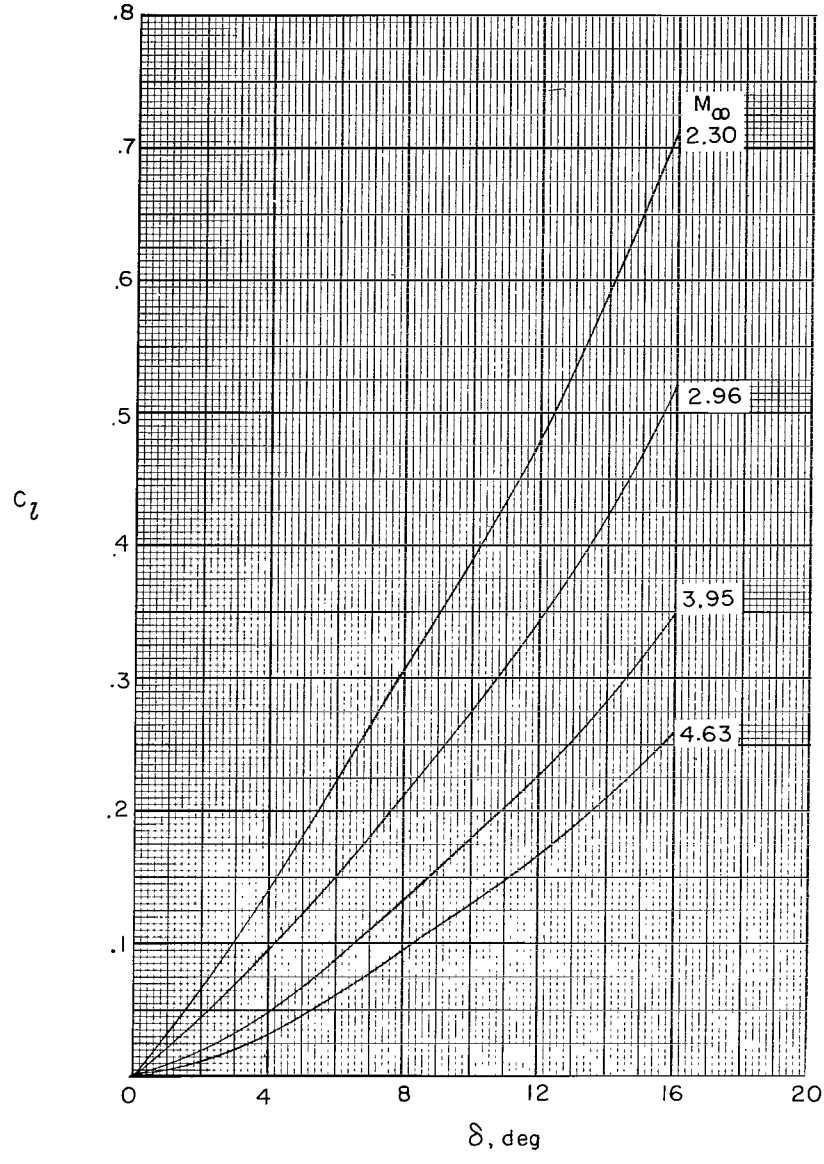

(b) c = 0.615.

Figure 10.- Continued.

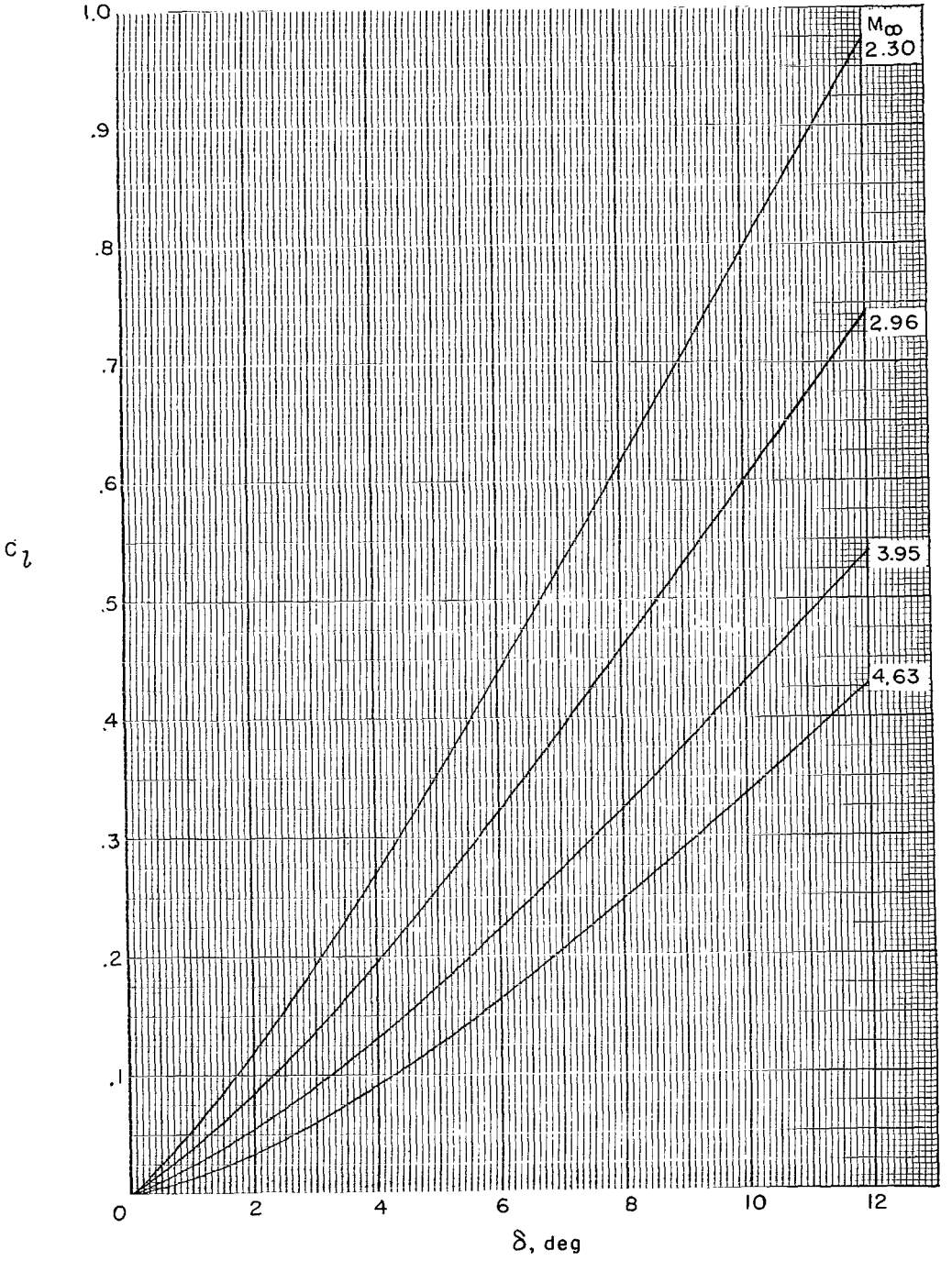

(c) c = 1.230.

Figure 10.- Concluded.

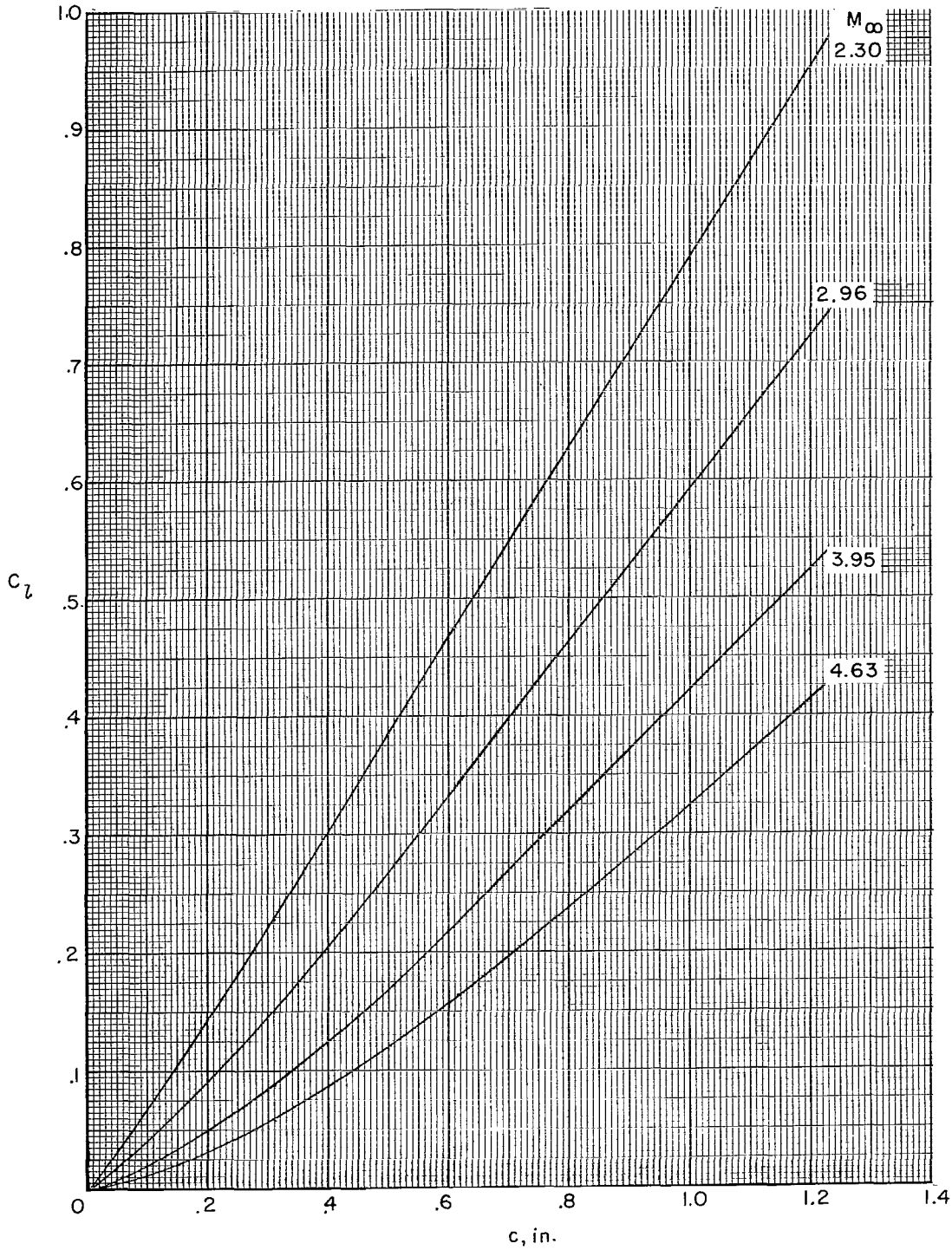

Figure 11.- Variation of rolling-moment coefficient with roll-control-tab wedge chord for $\delta = 12^{\circ}$.

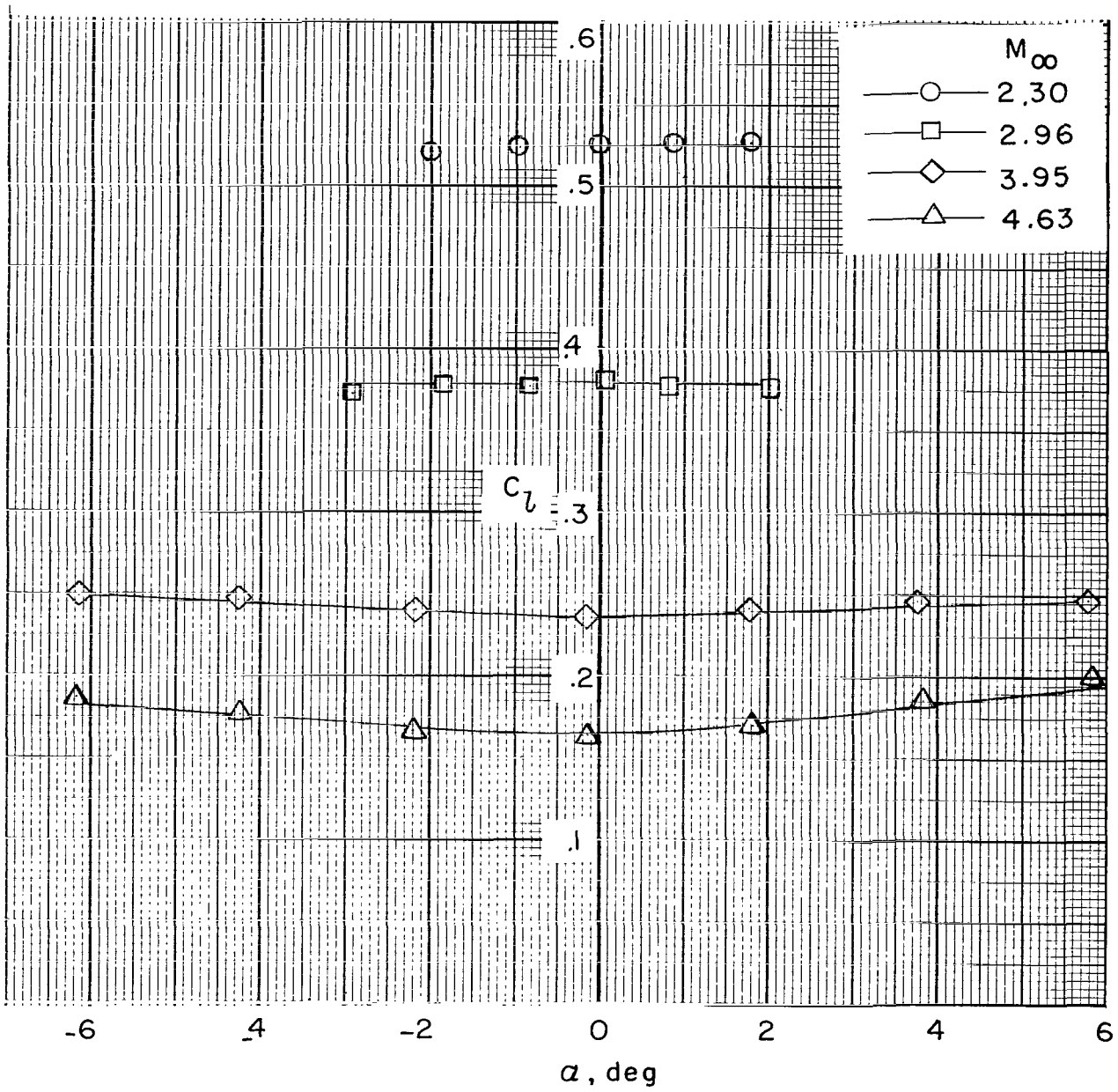

Figure 12.- Typical variation of rolling-moment coefficient with model incidence angle for roll-control tab $c = 0.308$, $\delta = 22^{\circ}$.

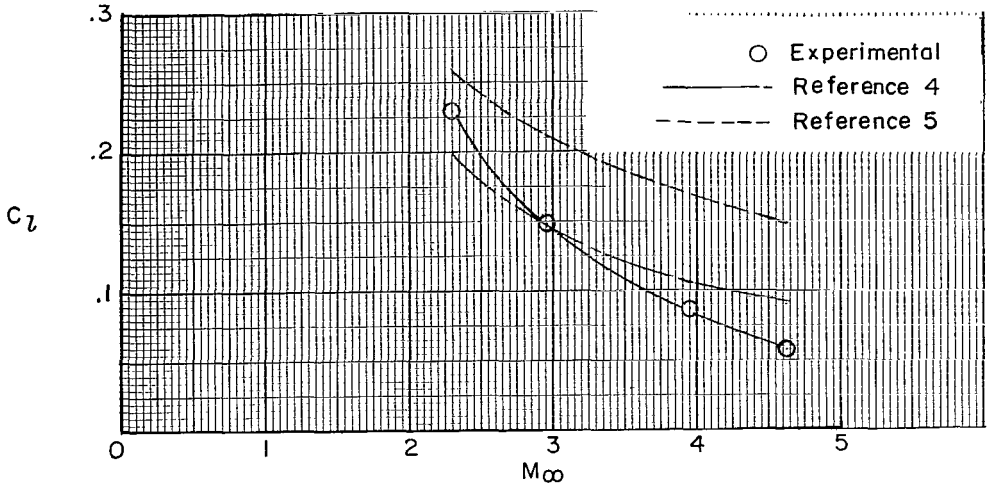

(a) $c = 0.308$; $\delta = 12^\circ$.

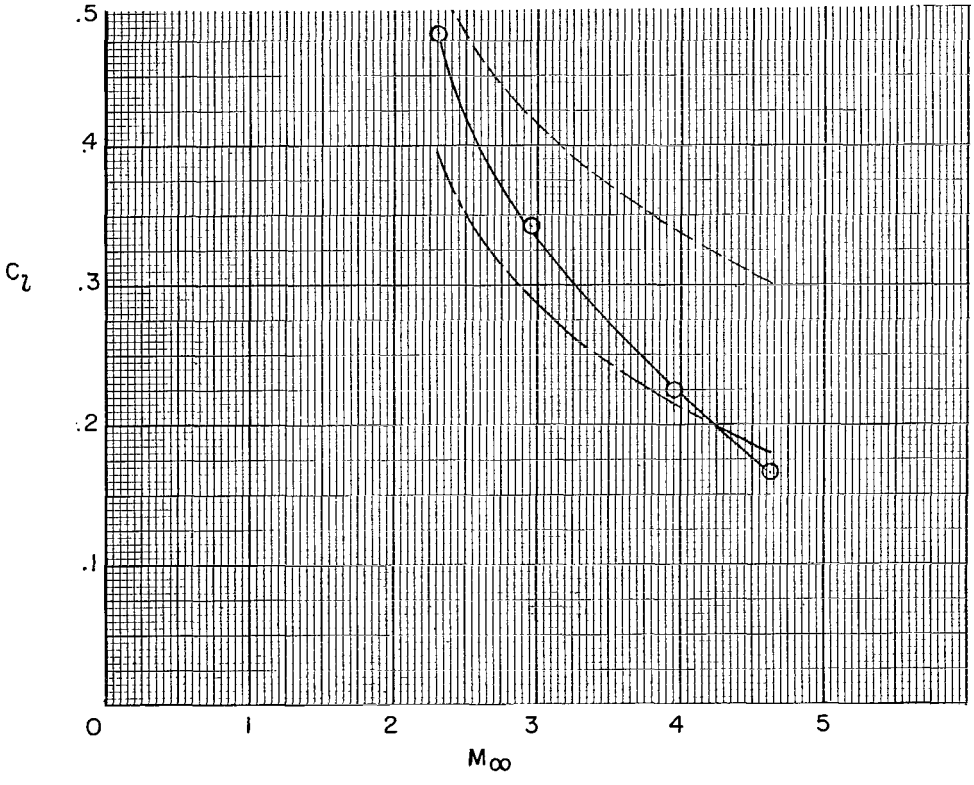

(b) $c = 0.615$; $\delta = 12^\circ$.

Figure 13.- Comparison of theory with experimental rolling-moment coefficients for δ of 12° and various roll-control-tab chords.

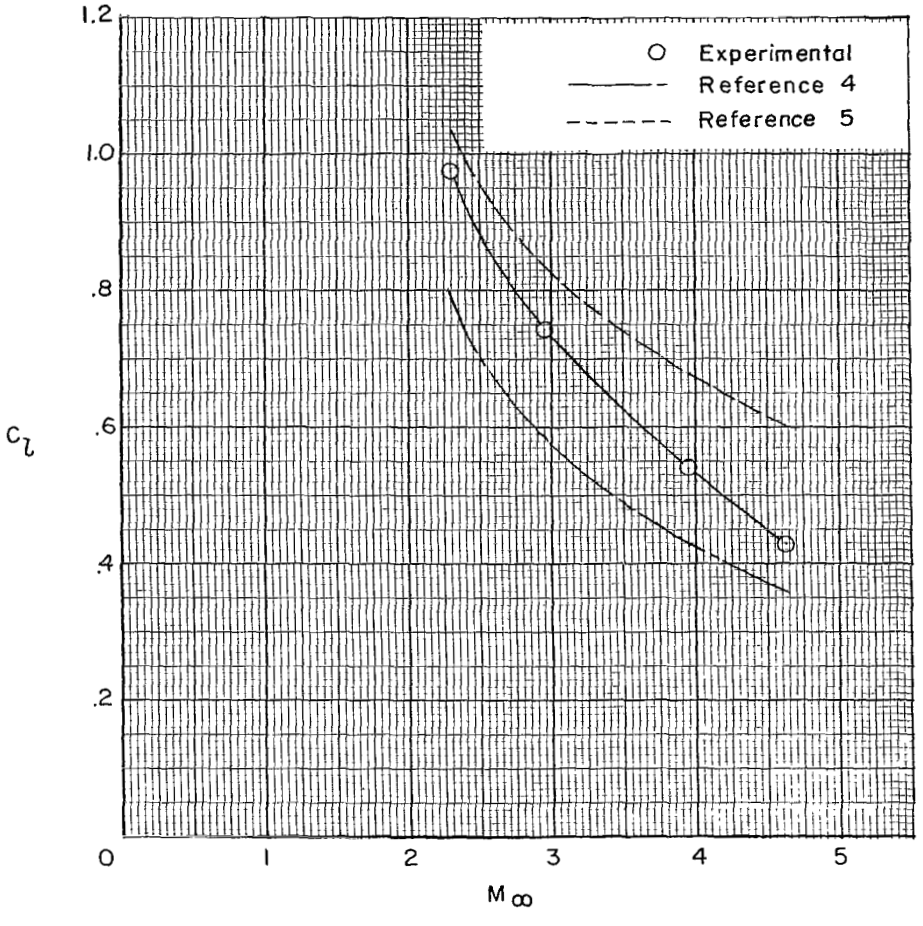

(c) $c = 1.230$; $\delta = 12^{\circ}$.

Figure 13.- Concluded.

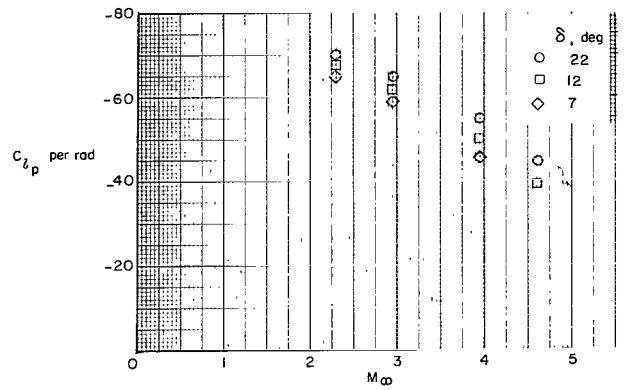

(a) c = 0.308.

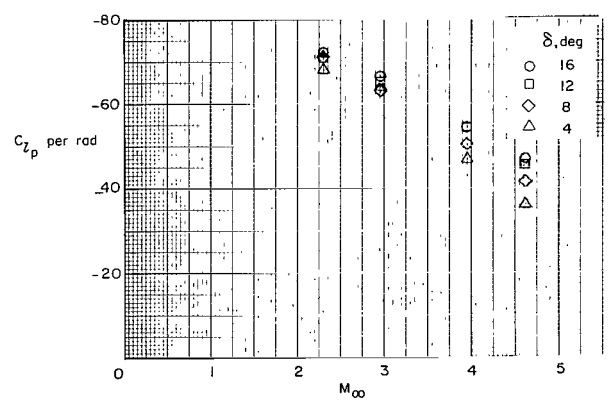

(b) c = 0.615.

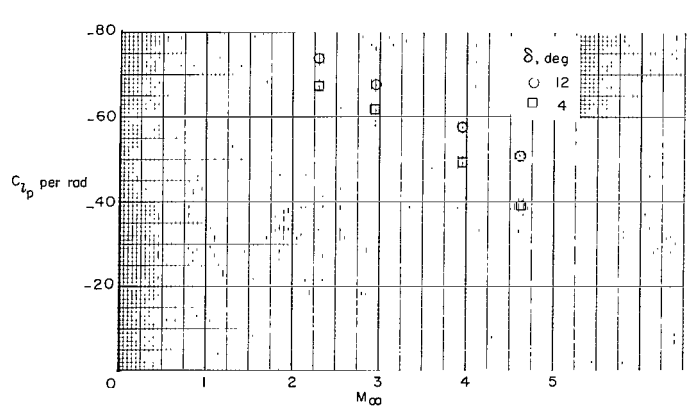

(c) c = 1.230.

Figure 14.- Variation of damping-in-roll parameter with free-stream Mach number for various roll-control tabs.

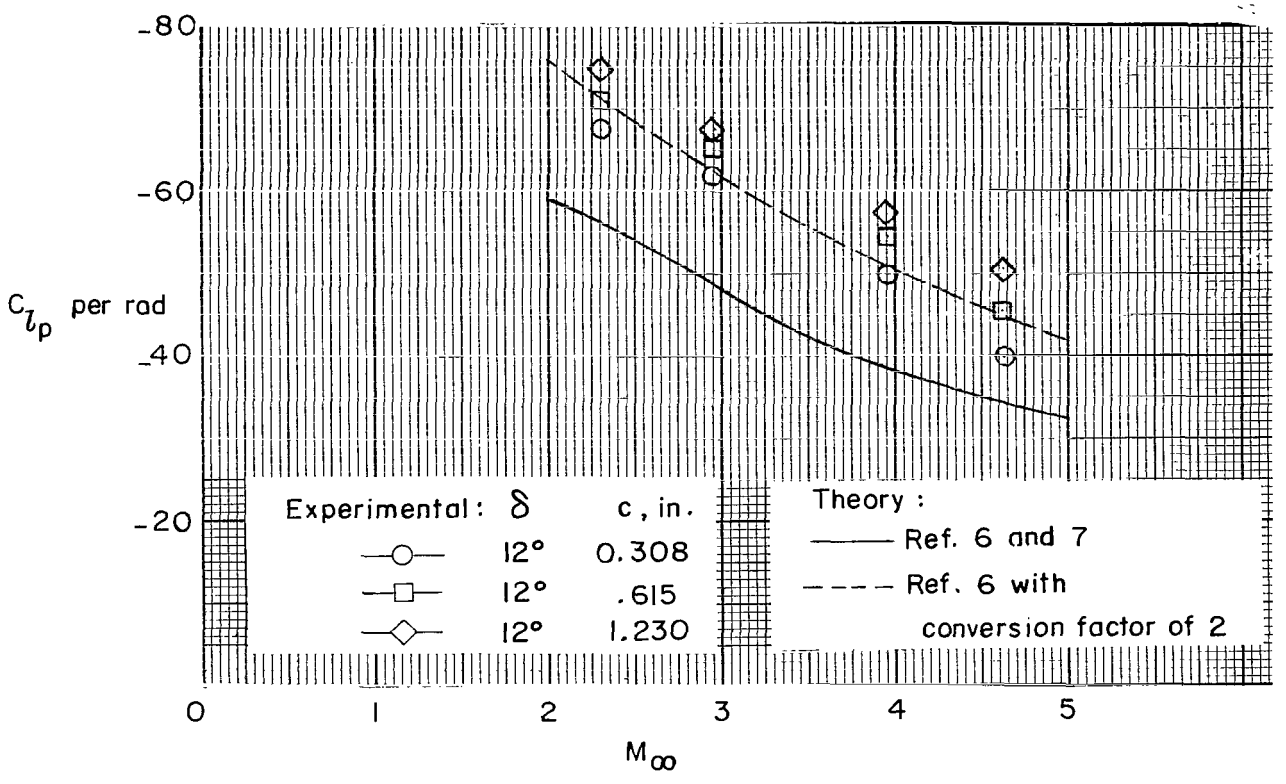

Figure 15.- Comparison of theory with experimental data.

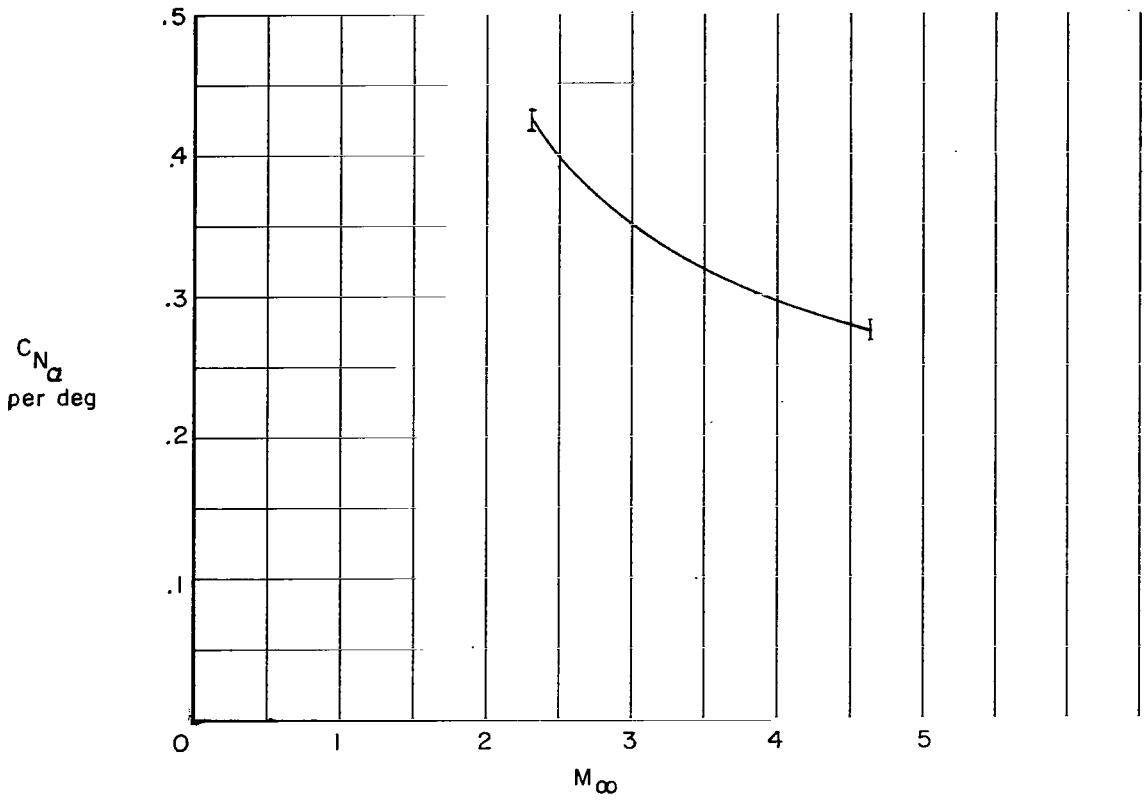

Figure 16.- Variation of model normal-force-curve slope with free-stream Mach number for all roll-control tabs. I represents spread in experimental data.

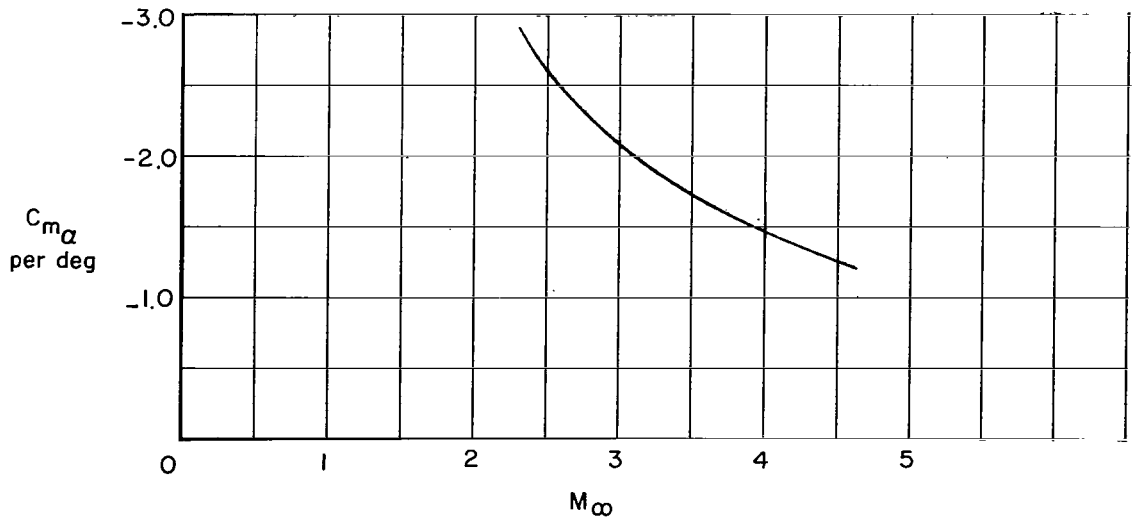

Figure 17.- Variation of model static stability parameter with free-stream Mach number for all roll-control tabs.

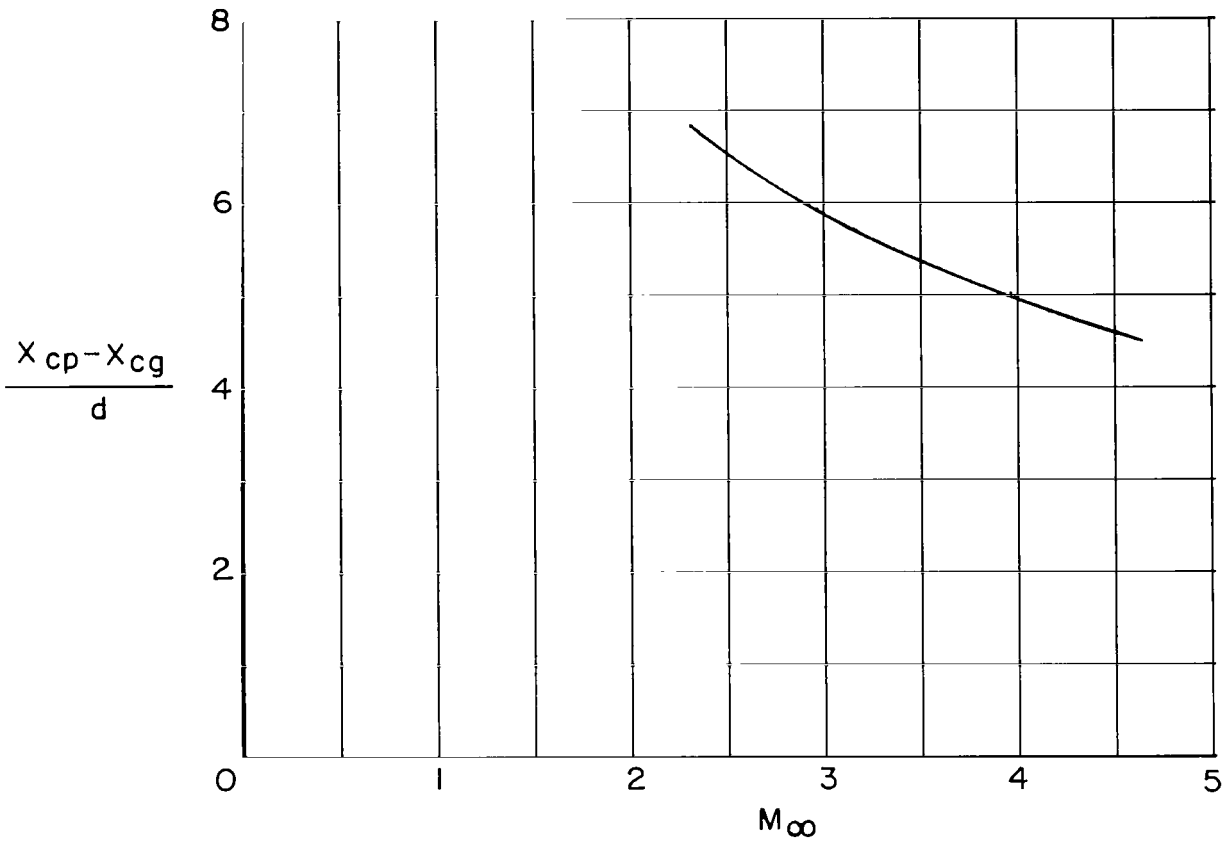

Figure 18.- Variation of model static margin parameter with free-stream Mach number for all roll-control tabs.

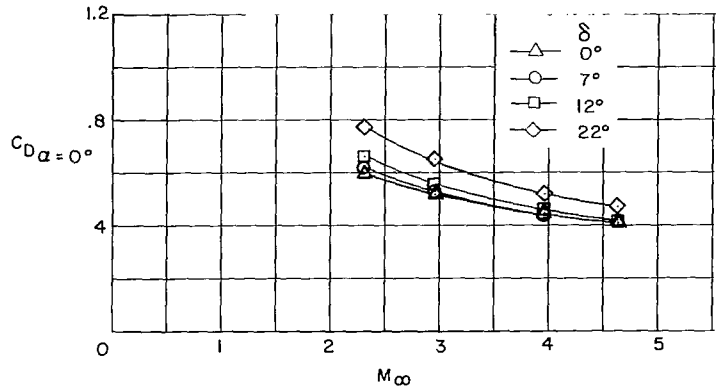

(a) c = 0.308.

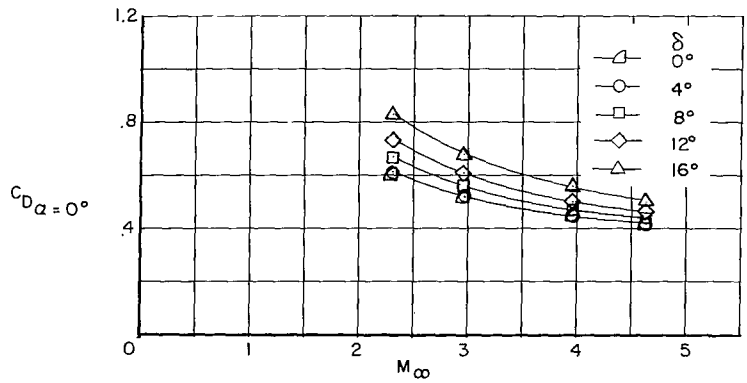

(b) c = 0.615.

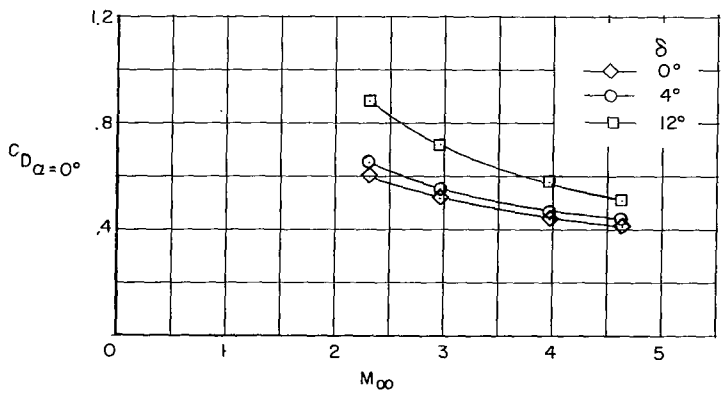

(c) c = 1.230.

Figure 19.- Variation of model drag coefficient (excluding base drag) with free-stream Mach number.

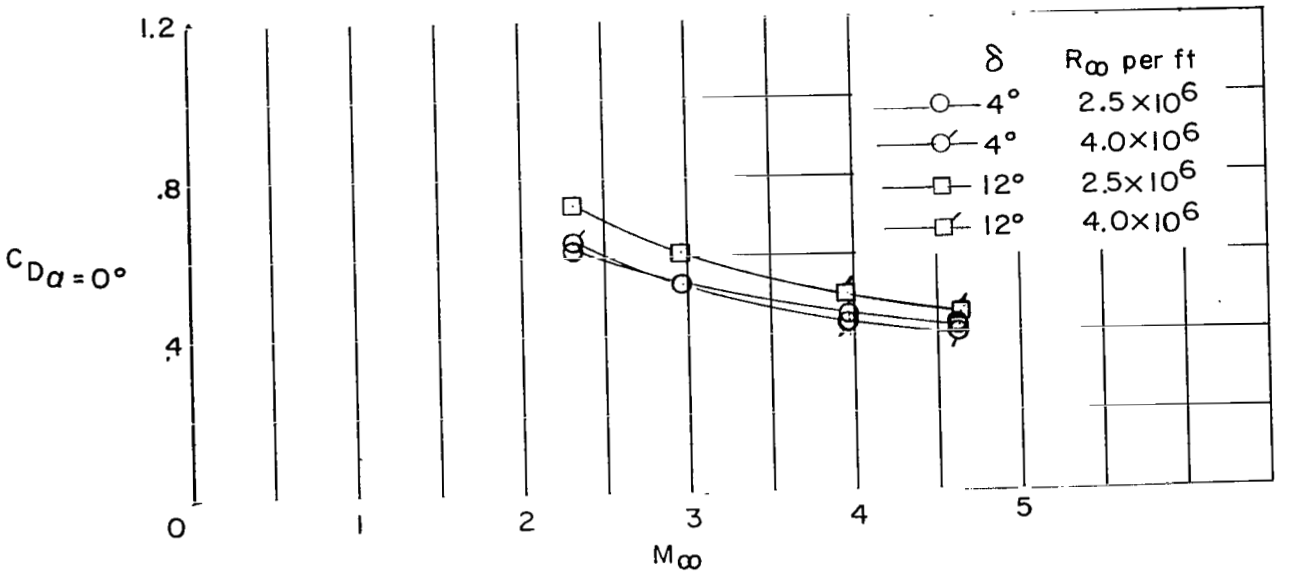

Figure 20.- Effect of free-stream Reynolds number on model drag coefficient for roll-control tabs of $c = 0.615$ and $\delta = 4^\circ$ and 12°.

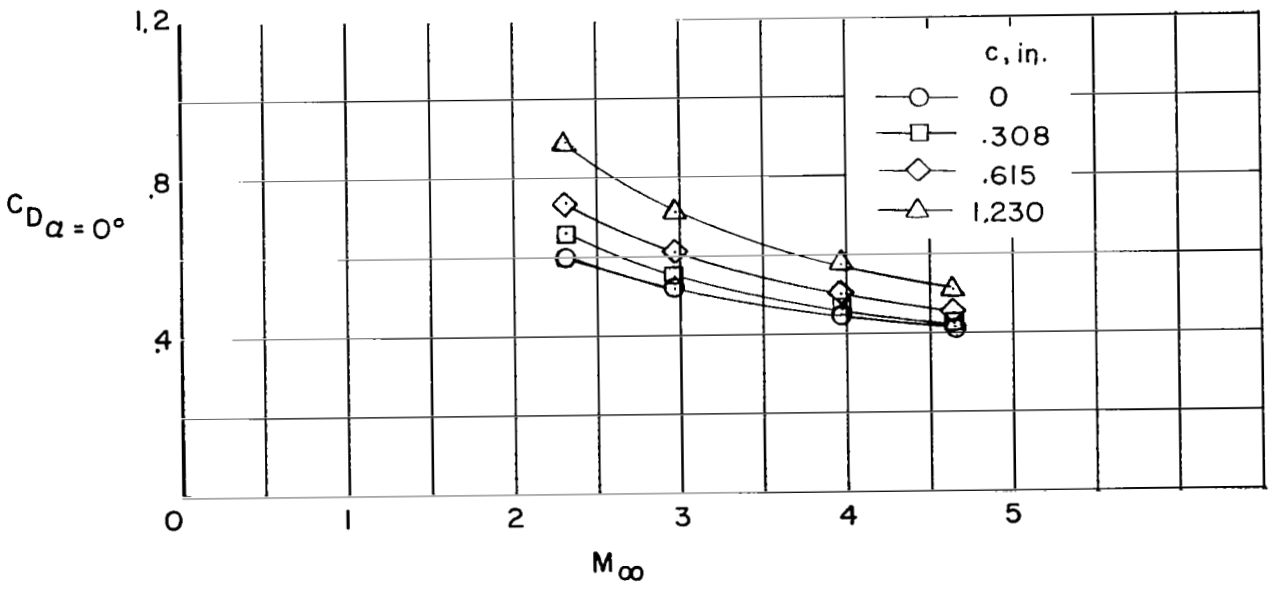

Figure 21.- Effect of roll-control-tab chord c on model drag coefficient for $\delta = 12^\circ$.

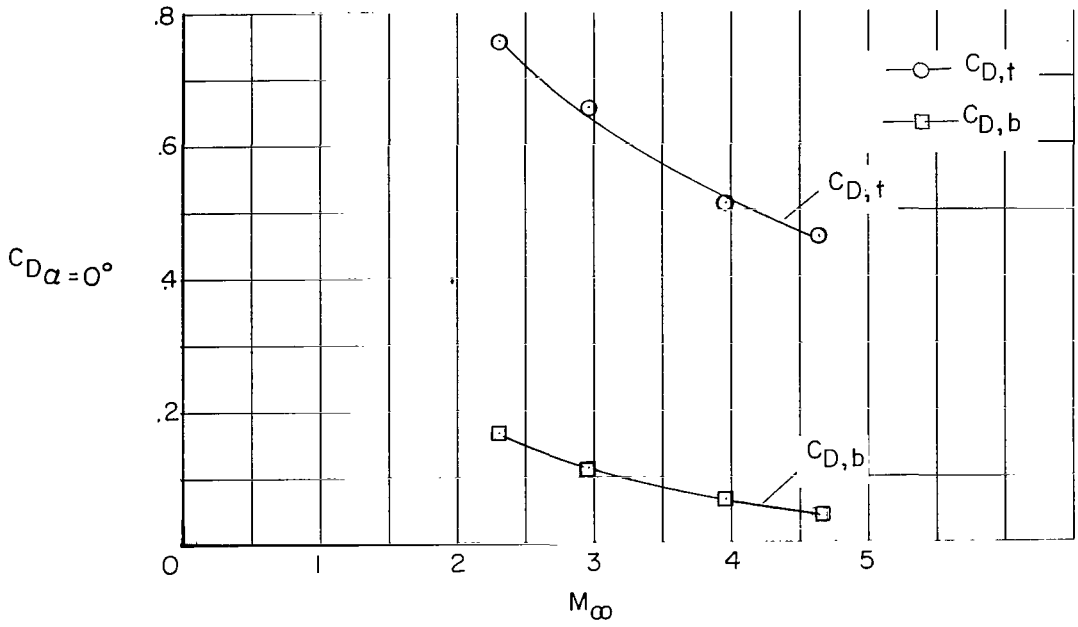

Figure 22.- Variation of model total drag coefficient and base drag coefficient with free-stream Mach number for $\delta = 0°$.

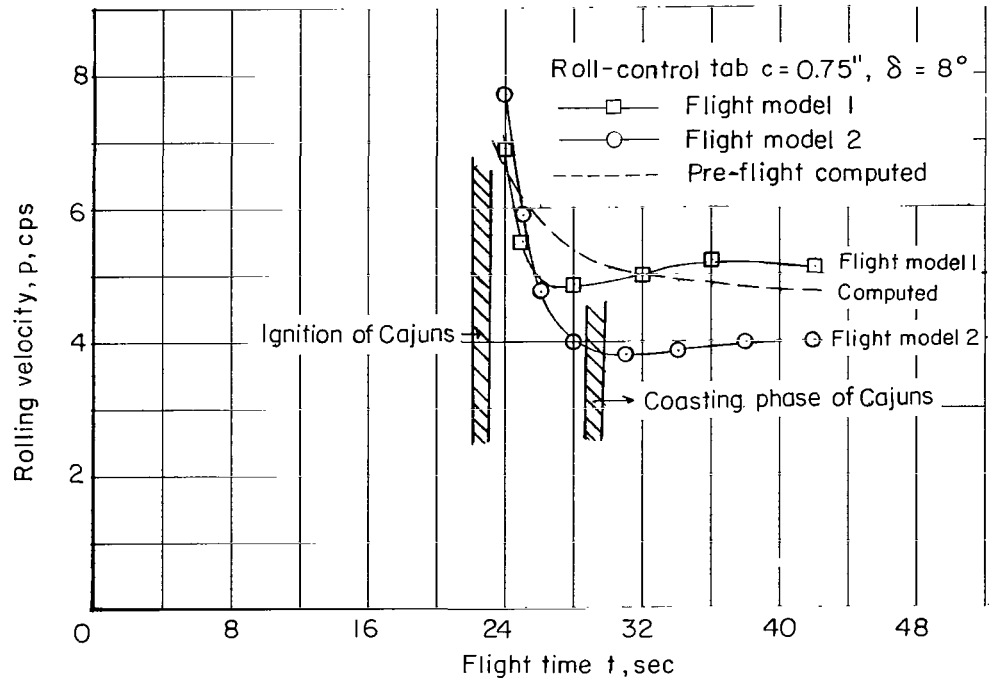

Figure 23.- Comparison of rolling velocity reduced from free testing Cajun stages with values obtained from preflight trajectory calculations using wind-tunnel data.

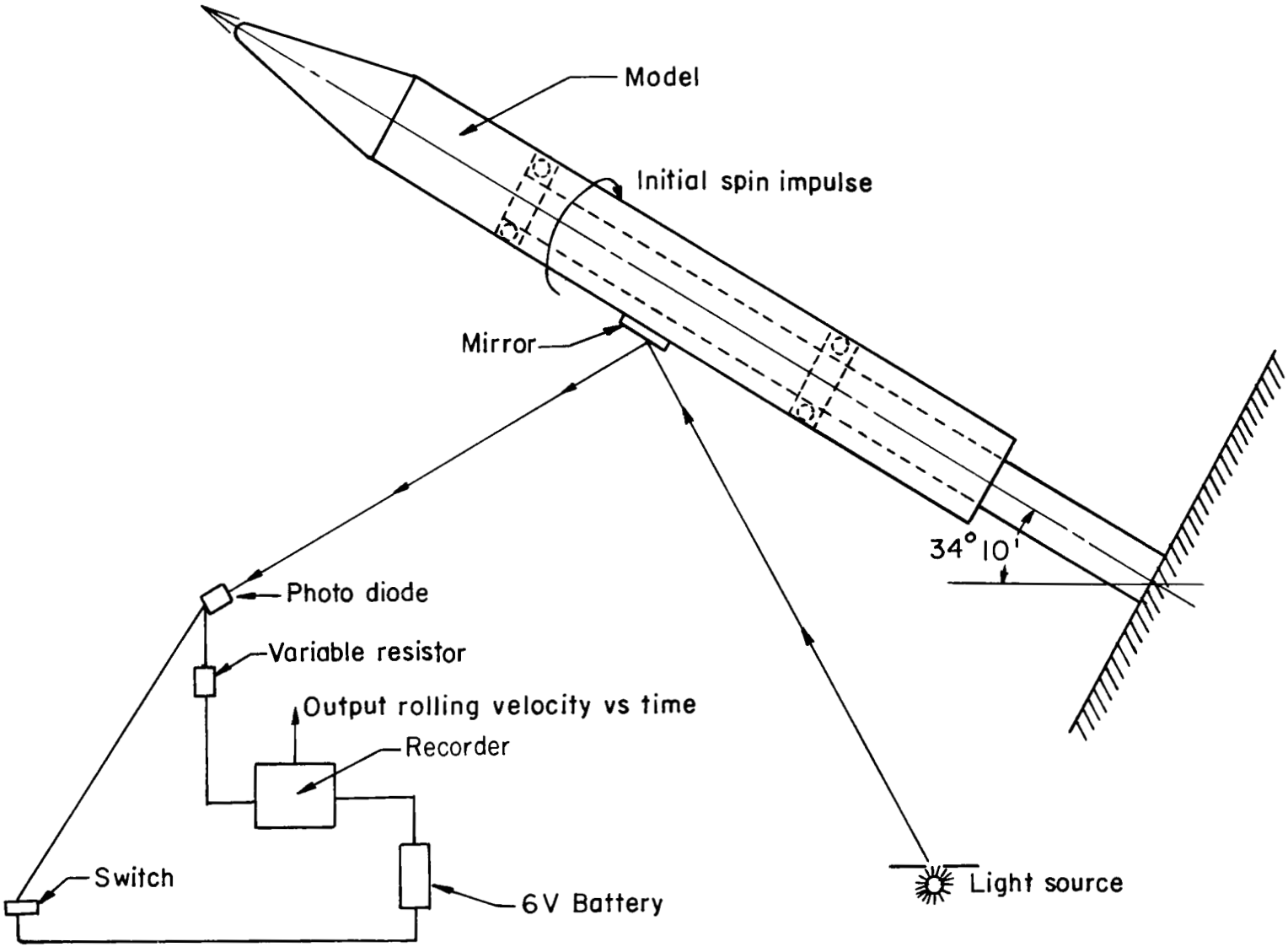

Figure 24.- Laboratory model setup and electronic equipment used to evaluate friction from ball bearings.

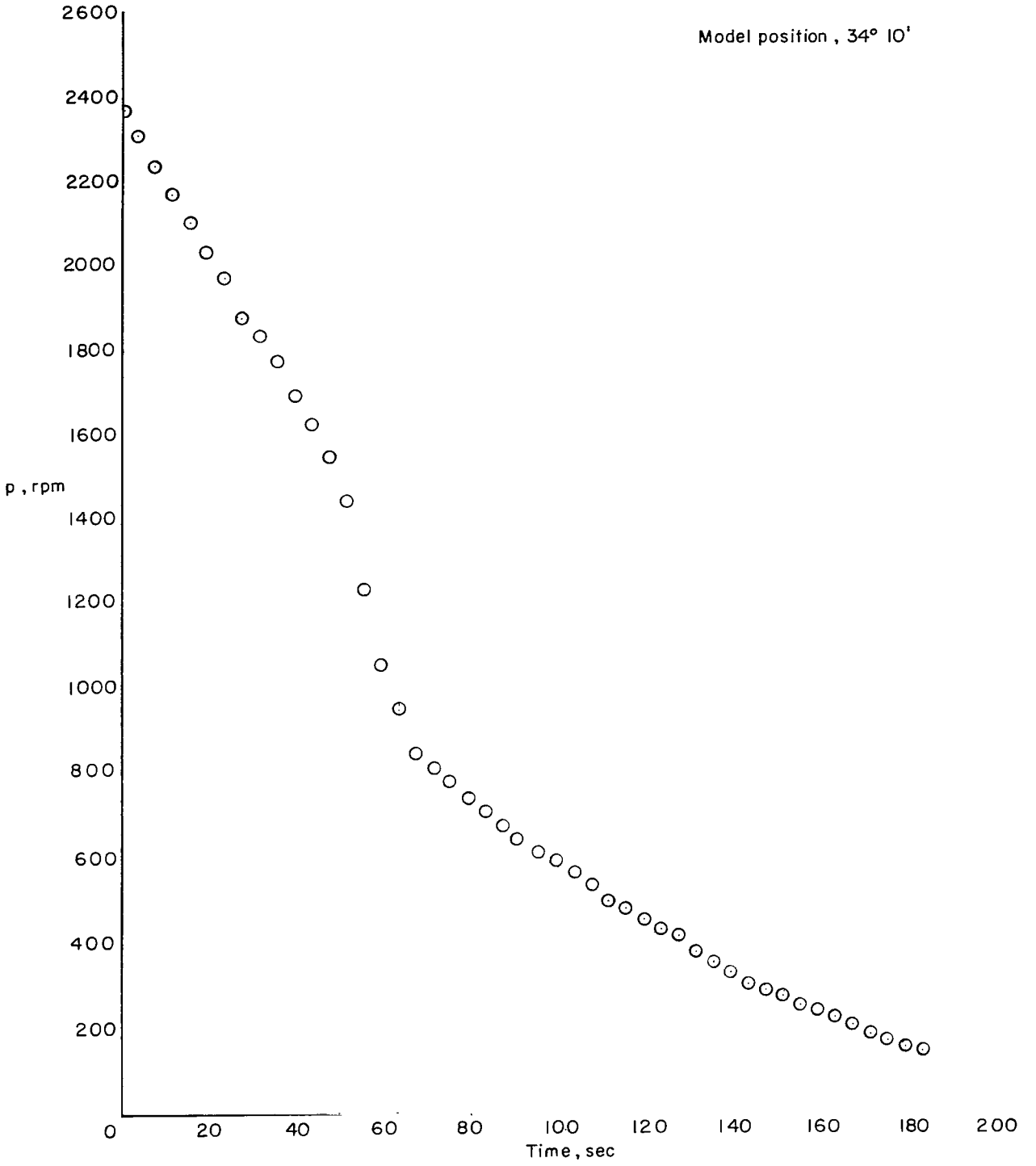

Figure 25.- Rolling-velocity—time history for model of Cajun stage without fins.

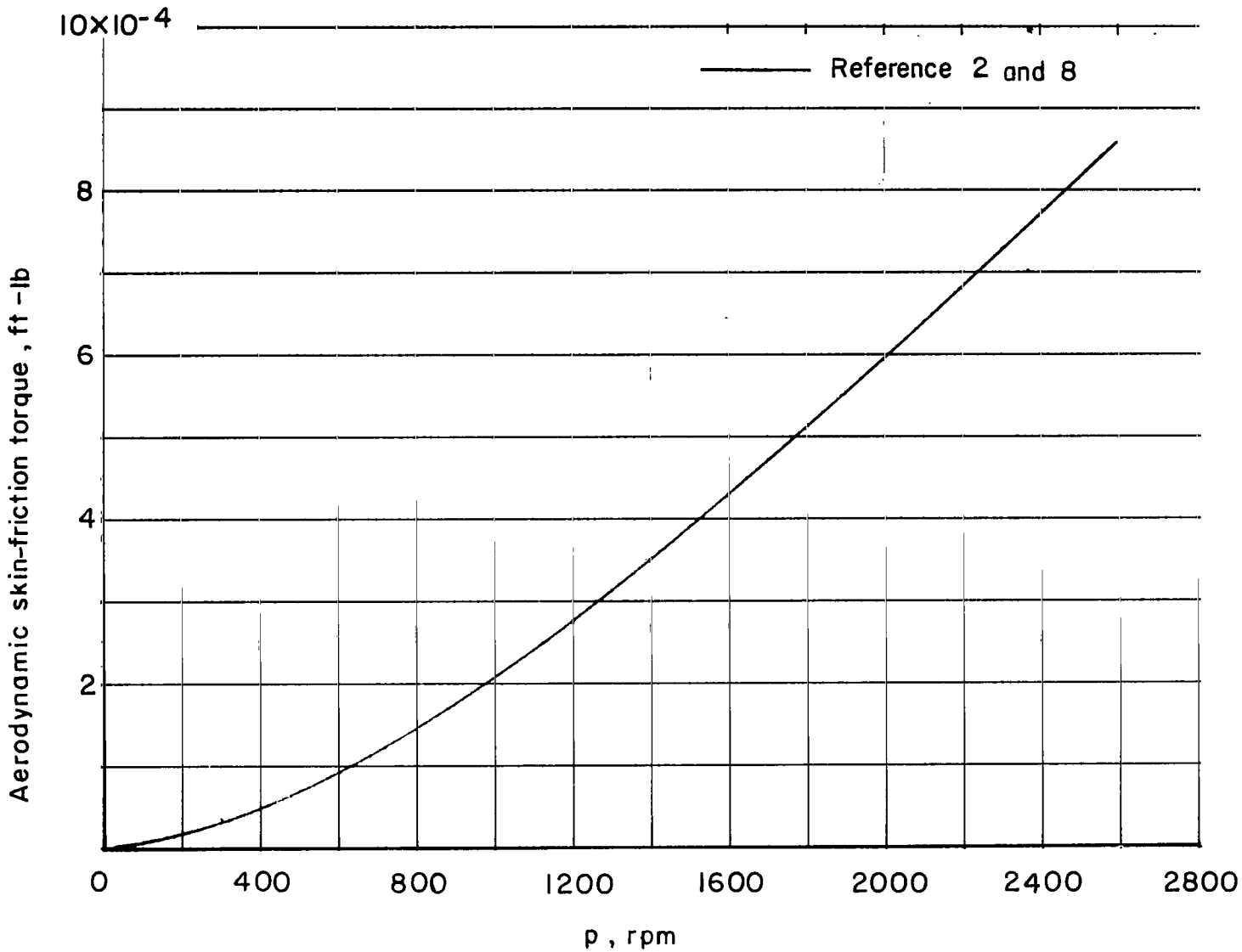

Figure 26.- Variation of aerodynamic skin-friction torque with rolling velocity for model of Cajun without fins.

NASA-Langley, 1965 L-4073

"The aeronautical and space activities of the United States shall be conducted so as to contribute . . . to the expansion of human knowledge of phenomena in the atmosphere and space. The Administration shall provide for the widest practicable and appropriate dissemination of information concerning its activities and the results thereof."

—NATIONAL AERONAUTICS AND SPACE ACT OF 1958

NASA SCIENTIFIC AND TECHNICAL PUBLICATIONS

TECHNICAL REPORTS: Scientific and technical information considered important, complete, and a lasting contribution to existing knowledge.

TECHNICAL NOTES: Information less broad in scope but nevertheless of importance as a contribution to existing knowledge.

TECHNICAL MEMORANDUMS: Information receiving limited distribution because of preliminary data, security classification, or other reasons.

CONTRACTOR REPORTS: Technical information generated in connection with a NASA contract or grant and released under NASA auspices.

TECHNICAL TRANSLATIONS: Information published in a foreign language considered to merit NASA distribution in English.

TECHNICAL REPRINTS: Information derived from NASA activities and initially published in the form of journal articles.

SPECIAL PUBLICATIONS: Information derived from or of value to NASA activities but not necessarily reporting the results of individual NASA-programmed scientific efforts. Publications include conference proceedings, monographs, data compilations, handbooks, sourcebooks, and special bibliographies.

Details on the availability of these publications may be obtained from:

SCIENTIFIC AND TECHNICAL INFORMATION DIVISION

NATIONAL AERONAUTICS AND SPACE ADMINISTRATION

Washington, D.C. 20546